Development of a spatial, dynamic, fuzzy fire risk model for Chitwan District, Nepal

Rob Burgess
March , 2011

Course Title:	Geo-Information Science and Earth Observation for Environmental Modelling and Management
Level:	Master of Science (MSc)
Course Duration:	September 2009 – March 2011
Consortium partners:	University of Southampton (UK) Lund University (Sweden) University of Warsaw (Poland) University of Twente, Faculty ITC (The Netherlands)

Development of a spatial, dynamic, fuzzy fire risk model for Chitwan District, Nepal

by

Rob Burgess

Thesis submitted to the University of Twente, faculty ITC, in partial fulfilment of the requirements for the degree of Master of Science in Geo-information Science and Earth Observation for Environmental Modelling and Management.

Thesis Assessment Board

Chairman: Dr. Y.A. Hussin
External Examiner: Dr. P. Pilesjö
Internal Examiner: Ms. Ir. L.M. van Leeuwen
Supervisor: Dr. M.J.C Weir

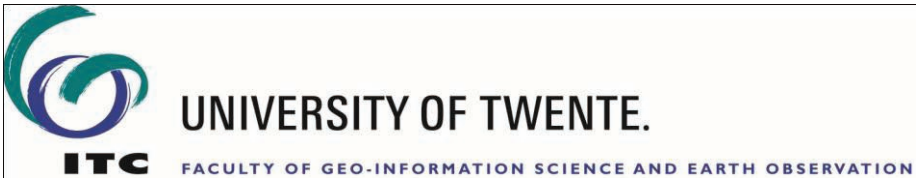

Disclaimer

This document describes work undertaken as part of a programme of study at the University of Twente, Faculty ITC. All views and opinions expressed therein remain the sole responsibility of the author, and do not necessarily represent those of the university.

Abstract

Wildfire can exacerbate forest degradation and accelerate land cover change. In developing countries such as Nepal, few resources are available to address these problems. This study aimed to develop a method that incorporates fuzzy logic on both spatial and temporal dimensions to identify regions of Chitwan District most at risk to wildfire occurrence. Fire risk factors were identified and grouped into five sub-models consisting of biophysical risk, ignition risk, weather risk, detection and response. Fuzzy membership functions were used to standardise factors based on the spatial patterns of a burn scar sub-set. The dynamic weather risk sub-model was standardised by applying fuzzy membership functions to monthly outputs of a drought index and average temperature. Convex (weighted) combination was used to combine variables within each sub-model, and to combine sub-models to produce monthly outputs. A second sub-set of burn scars was used to validate the model, before a sensitivity analysis was performed. Spatially, risk was highest in areas characterised by agriculture and grassland, while areas of lowest risk were located in remote, high altitude forests. The dynamic aspect of the model showed that April and September were the highest and lowest risk months respectively. The relative operating characteristic was used to validate these outputs, and AUC ranged between 0.7 and 0.78. This dynamic aspect of the model was successful because it identified the highest risk month as April, which is traditionally the month of greatest fire activity, while September was identified as the lowest risk month, which is typically towards the end of the monsoon season. However, the range in risk values between the highest and lowest risk months was not as great as expected. The overall aim of developing a spatial, dynamic, fuzzy fire risk model for Chitwan District, Nepal, was achieved, but the methods used here are not without their limitations.

Keywords: fire risk, fuzzy logic, multi-criteria evaluation, pairwise comparison, relative operating characteristic, Nepal.

Acknowledgements

I would like to take this opportunity to thank the many people who made this thesis possible.

I am very grateful to Dr. Michael Weir whose support, guidance and attention to detail, from the initial to the final stages, enabled me to complete this study and develop skills essential for the future.

I would also like to show my gratitude to Dr. Yousif Hussin for the considerable time he spent organising and coordinating fieldwork, as well as the advice given both in the field and in our weekly group meetings.

When in Kathmandu, the staff of the International Centre for Integrated Mountain Development (ICIMOD) were very helpful. In particular, thanks to Dr. Amarnath Giriraj and Hammad Gilani for provision of data related to my study area, as well as organising fieldwork logistics.

I am also indebted to Srijana and Shyam for their invaluable help during fieldwork, especially with regard to their linguistic talents, without which achieving my objectives would have been much harder. Thanks also to our helpers, our driver Bidur who took me to all the locations I needed to visit, and to the community of Shaktikhor.

Thanks to all my friends on the NRM course who worked in room 4-036 who were very helpful and kind.

Finally thanks to all my friends on the GEM course with whom I have enjoyed being with for the past 18 months, and with whom I share many great memories.

Table of contents

List of figures

List of tables

1. INTRODUCTION

1.1. Background

1.1.1. Fire and wildfire

Throughout history, fire has been an essential part of human life. In his book *The Descent of Man*, Charles Darwin describes the discovery of fire as "probably the greatest ever made by man, excepting language" (Darwin, 1882, 49). Fire enabled humans to become more successful by generating heat and light, enriching diets through cooking, and warding off predators (Wrangham and Carmody 2010). Control of fire also allowed man to influence the surrounding landscape. For example, hunter-gatherers have used and continue to use fire successfully in the control of wildlife and to clear land for habitation (Bowman *et al.* 2009).

Of course, fire was present in the landscape long before man learned to master it. Wildfire, for example, remains an essential aspect of many ecosystems from the savannas of Africa to the tropical rainforests of Latin America. In recent history, however, humankind's increasing dominance over the environment has led to the expansion of agricultural and urban land into previously undisturbed environments prone to wildfire (Bowman *et al.* 2009). Despite efforts to control wildfire, management strategies are imperfect. Wildfire therefore remains a significant issue, posing a variety of problems to those concerned, from government officials and fire managers, to those that live within the fire affected areas.

1.1.2. Problems caused by wildfires

Whether natural or human caused, wildfire can be a catastrophic phenomenon responsible for burning millions of hectares globally every year, and causing billions of dollars of damage (Cochrane 2002). It is a problem that receives considerable attention in developed countries, such as the US, Canada, Europe and Australia where much research has been done into the issues that surround wildfire. However, wildfire is also an issue affecting developing countries such as Nepal, which has recently been dubbed a "white spot" by the IPCC as so few studies have been conducted (Khadka 2009).

Fire is a significant cause of environmental degradation (Stickler *et al.* 2009). Forests become fragmented as trees are damaged or destroyed, not only leading to a loss of biodiversity as habitats are degraded, but exposing the underlying soil to

processes of erosion. The combination of these aspects gives rise to land cover change, whereby previously undisturbed forests are converted to grassland or scrub ecosystems (Matricardi *et al.* 2010; Eva and Lambin 2000).

Despite disturbed landscapes being at an increased risk of further fire events, land cover change can also contribute to the wider issue of climate change. For example, at a regional scale, Mölders and Kramm (2007) observed that the loss of vegetation cover can alter surface roughness and albedo, affecting the energy flux between the surface and atmosphere. They then go on to suggest this can alter local weather patterns, affecting cloud formation and precipitation. Amiro *et al.* (1999) also observed that burned area remained warmer than undisturbed forest for up to 15 years after a fire event, indicating that fire can impact climate at a local scale.

Globally, biomass burning has been a significant source of carbon dioxide and other greenhouse gases. Of 8,700 Tg of biomass burned annually, including forest cover, 3,500 Tg of carbon is released as carbon dioxide (Palacios-Orueta *et al.* 2005). Change in this forest cover accounts for approximately 20 - 25% of the total amount of carbon released from human activities every year (Dowmoh *et al.* 2009). This emission contributes to climate change both directly, through release of greenhouse gas from combustion, and indirectly, through loss of vegetation which would have otherwise sequestered carbon. Flannigan *et al.* (2000) suggest that potential therefore exists for a feedback mechanism whereby release of greenhouse gas forces a change in climate, which facilitates conditions that promote an increase in fire frequency.

1.1.3. Fire hazard and risk

Within the fire literature there are numerous definitions of the terms fire hazard and fire risk, and it is important to distinguish among them. The term hazard, in its most basic sense was defined by Burton and Kates (1964, 413) as "those elements in the physical environment which are harmful to man and caused by forces extraneous to him". Based on this definition, the wildfire itself would be the hazard. However, Bachmann and Allgöwer (2001) discuss how using the term 'fire hazard' shifts the focus away from the wildfire process, and onto specific elements of the fire environment that could potentially contribute to fire behaviour or severity. For example, the US National Wildfire Coordinating Group (NWCG), focuses solely on fuel complexes as a hazard, "defined by volume, type, condition, arrangement, and location that determines the degree of ease of ignition and the resistance to control" (NWCG 2003).

Fire risk differs from fire hazard in that it includes the components of probability and potential damage. In Hall (1992, 131), risk is defined as "*a*), a type and degree of danger or peril or loss; and *b*), the relative likelihood that that type and degree of danger will occur". A similar definition of wildfire risk is proposed by Bachmann and Allgöwer (2001, 28): "The probability of a wildland fire occurring at a specified location and under certain circumstances, together with its expected outcome as defined by its impacts on the object it affects". The above definitions of fire risk do, however, emphasize the destructive and sometimes negative impacts of wildfire. This may not be an accurate definition if coming from the standpoint of individuals who use fire to manage ecosystems. In this situation, Hardy (2000, 81) argues that the "emotional and value-driven" terms used to describe damage, such as 'catastrophic', be excluded from the fire management vernacular.

1.1.4. Role of remote sensing within fire research

Since the launch of the first Landsat satellite in 1972, remote sensing has proven to be a major benefit to many disciplines, from land cover mapping to water resource management. Application of remotely sensed data to fire related issues is no exception, and has provided many benefits. Satellites are capable of sampling a large spatial extent on a regional or even global scale that would simply not be possible on the ground. Furthermore, this data generally is obtained at relatively low cost when compared to their ground-based equivalents. Another major advantage of remotely sensed data is that it can be used to develop fuel maps, provide topographical information and estimate weather aspects that together affect fire (Chuvieco 2000).

Remote sensing also fulfils a significant role in the near real-time monitoring of current fire events, including both detection of active fires, and post-fire assessment of burned area. A number of satellites have been used in the detection of active fires. The GOES satellite, for example, has a revisit time of approximately 15 minutes, meaning that fire activity can be tracked in detail (Prins and Menzel 1992). However, a major drawback is GOES's coarse resolution of 4 km, as only the largest of fires can be detected. In contrast to the GOES satellite, Landsat's high resolution of 30 m has provided the opportunity to identify individual fires, but is limited by a revisit time of 16 days (Chuvieco and Congalton 1989). AVHRR provides a trade-off between the spatial and temporal resolution. Fires greater than a 1 km^2 are revisited every 24 hours, and was used extensively within the research community in the 1990s (Kaufman *et al.* 1998). Within the last decade, MODIS has replaced AVHRR in the detection of active fire. Its fire detection algorithm is, however, based on that used within AVHRR. This algorithm functions largely around the mid-

infrared channels (3.75 μm), which are highly sensitive to the elevated radiance that is emitted by active fire. A fire is detected when radiance within a pixel is greatly elevated above the radiance of the surrounding (background) pixels (Justice 2002).

Satellite remote sensing also provides "one of the only means of monitoring burned vegetation on a regional or global scale" (Roy 2005, 138), and much data has been used in the development of methods to identify and quantify this burned area. Some of these methods rely simply on a visual interpretation of a satellite image. For example, satellites such as Landsat, SPOT and ASTER provide high resolution imagery from which burn scars can be digitised. Band combinations from satellite sensors also exist which aim to maximise the ability of the analyst to distinguish between burned and unburned areas. Burned areas typically have a low reflectance against the relatively high reflectance of the surrounding vegetation. SPOT and Landsat data have also been used to develop indices that identify burned area. The Normalised Burn Ratio (NBR), for example, exploits the near-infrared (NIR) and mid-infrared (MIR) regions of the spectrum. When a fire occurs, reflection in the NIR decreases as vegetation is lost, but reflection in the MIR increases because soil moisture content is burned and hence absorbs less radiation (Key and Benson 2006). NDVI is also commonly used in the detection of burned area. The differenced NDVI (dNDVI) method involves calculating the NDVI of the fire affected area both before and after the fire event. The post-fire NDVI is then subtracted from the pre-fire NDVI, which enables not only the burned area to be located, but also an assessment of the degree of damage caused by the fire (Fox *et al.* 2008).

1.1.5. Importance of forests in Nepal

As mentioned in section 1.1.3, wildfire is an issue that affects the developed and developing world, including countries like Nepal. This section highlights the importance of forests in this country and also describes how forest is managed today. The following section discusses the threats these forests face from wildfire.

Forest covers approximately 30% of Nepal's land area. This is important in a country characterised by steep slopes, where an absence of forests would encourage slope instability and erosion of top soils. Acharya and Dangi (2009) estimated that in regions of high altitude, maintaining 1 ha of paddy land required 50 ha of forest and grazing land. Fuel wood is still a major source of energy in Nepal. In 2002, 76% of energy consumed was provided by fuel wood (Pokharel 2007).

Forests also have significance for rural communities. Prior to the 1970s, forests were managed solely by government forestry agencies. However, in the 1970s, there was a drive to include also public participation within forest management (Timsina 2003). This meant that the rights of access, use, exclusion and management were passed over to local communities (Thom 2008). These are known as community forest user groups (CFUGs), and are important for supporting livelihoods, as well as conserving the forests and tackling deforestation.

1.1.6. Wildfire in Nepal

Nepal's forests have faced and continue to face threats from deforestation and degradation. One species in particular, Sal (*Shorea robusta*), is an economically important deciduous species common to the sub-tropical south of the country, also known as the Terai region. On the one hand, Sal has been subjected to widespread logging due to its desirable hardwood properties, while on the other, wildfire has promoted degradation of it and other forest species. This has accelerated the rate of land cover change. For example, from the 1970s through to the 1990s, degradation of forestland into shrubland was occurring at a rate of 5.5% per year (Acharya and Dangi 2009), with deforestation for agriculture progressing at 1.3% per year (Rautiainen and Suoheimo 1997).

As mentioned, wildfire predominantly occurs within this Terai region, with districts such as Chitwan, Nawalparasi and Palpa particularly badly affected (ICIMOD 2010). Fire frequency is greatest throughout the period March, April and May. The weather during this time is characterised by low precipitation, high temperatures and strong winds. In March 2009, powerful fires flared, and 1,583 active fires were detected throughout the Terai belt. Thousands of hectares of forest and croplands were destroyed (ICIMOD 2010).

Fires have consequences for the communities around which they burn. The majority are of anthropogenic origin, used for land clearance purposes. However, these fires can frequently become difficult to control, particularly in periods of drought. Not only do these fires burn into adjacent fields, but also into surrounding grassland, forest and settlements (Acharya and Dangi 2009).

Attacking wildfires once they have started is essential in protecting the most vulnerable resources. However, Nepal is characterised by steep, often inaccessible terrain, limiting the capability of authorities to tackle fire. Road access is especially

limited. Attacking fire from the air is an effective way of controlling fires, but Nepal has few aircraft that can adequately achieve this.

Other methods that enable the wildfire issue to be tackled without the need for the expensive human intervention described above, and that are suitable to the Nepali context, should therefore be explored. The next section justifies a fire risk model approach that would enable authorities to manage the landscape to reduce the likelihood of a fire igniting and propagating in the highest risk areas.

1.2. Justification for fire risk model

In order to reduce the number of fires, or to ensure their effective control, it is necessary to have an understanding of which areas are most prone to fire damage (Chen *et al.* 2001). Fire risk modelling is one such approach that can achieve this. However, authorities in Nepal have limited access to relevant fire risk models and are therefore unable to effectively allocate resources because identification of the most vulnerable areas remains a challenge. The Intergovernmental Panel on Climate Change (IPCC) also recently dubbed the Nepal region as a "white spot", as so few studies have been conducted, and little data is available (Khadka 2009). Authorities therefore have few opportunities to develop and apply models specific to their region, again hampering efforts to develop effective fire risk models.

A further justification for a fire risk model is linked to the Reduced Emissions from Deforestation and Degradation in developing countries (REDD). Approximately 20% of global greenhouse gas (GHG) emissions are released through deforestation and degradation (Ohja *et al.* 2008). A fire risk model would enable forestry authorities to implement management strategies that reduce the quantity of fuel within a high risk area. This would contribute to the REDD programme as reducing fire risk could potentially reduce fire frequency, and hence the volume of emissions emitted by deforestation and degradation. It could also benefit rural communities because the more carbon that is stored within CFUGs, the greater the payment they receive from the REDD programme.

1.3. The fire environment

In order to understand the factors contributing to fire risk, it is necessary to examine the fire environment. Countryman (1972, p12) defines the fire environment as the "surrounding conditions, influences, and modifying forces" that determine the behaviour of a fire. Topography, fuel and weather are three major aspects of this, and form the three sides of the 'fire environment triangle'. The fire environment can

also be affected to a significant extent by human activity, such as the reduction of fuel quantity. It is important to consider also that, although the fire environment affects fire behaviour, in some situations large fires can interact with the environment itself, especially with respect to fuel.

1.3.1. Topography

Topography forms a significant aspect of the fire environment, with both direct and indirect effects on the potential fire behaviour. In a general sense, 'topography' - or features of the landscape - can not only promote extreme fire behaviour through the existence of 'chutes' or 'chimneys', but also present barriers to fire propagation with presence of lakes, bare soil or rocks. More specifically, fire behaviour is controlled by slope, elevation and aspect.

Slope is defined as the rate of change in elevation. Typically measured in degrees or percent, slope can directly affect fire behaviour due to its influence on a fire's rate of spread and flame length (Finney 1998). Fire burns rapidly uphill as radiant heat from the approaching flames reduces moisture content of adjacent fuel, raising it to ignition temperature (Rothermel 1972). Thermal energy released by the fire also creates a convection column of rising air, which aids fire movement in the up-slope direction. The convection column can also increase the risk of 'spotting', a process whereby release of firebrands into the atmosphere may result in ignition in other locations

Elevation above sea-level affects general climate characteristics. Lower elevations are typically characterised by higher temperature, and lower relative humidity. At high elevation, the effect of orographic rainfall is more pronounced to the extent that relative humidity and fuel moisture are greater, restricting the ability of fire to ignite or propagate (Romme and Knight 1981). In some locations, a thermal belt can exist in the mid-slope region, where the inversion layer contacts the mountain slopes (Pyne *et al.* 1996). Highest average temperatures are located here, and this explains why fires may burn on the mid-slope region, and not above or below this. Elevation also influences periods of seasonal snow melt, as snow packs at high elevation will be present for long periods, and when melting occurs fuel moisture content will be significant.

Aspect is the direction that a slope faces, and is measured in degrees from 0° (north), through to 180° (south) back to 360° (north). Flat surfaces are given the value of -1°. Southern facing slopes (in the northern hemisphere) are exposed to the greatest quantities of solar radiation. Furthermore, in the northern hemisphere south

and south-west facing slopes are exposed to the prevailing winds. The combination of these two results in higher temperatures, lower relative humidity and higher fuel quantities on southern facing slopes (Heyerdahl *et al.* 2001; Pyne *et al.* 1996). The opposite is true for north facing slopes.

1.3.2. Weather

Weather is the most dynamic element within the fire environment, and is the dominant factor that determines the degree of fire risk on a given day. It is important to distinguish between weather, which is the day to day variation in atmospheric conditions, and the climate, which is responsible for long-term weather patterns. The atmospheric conditions that influence fire are temperature, precipitation, wind and humidity, with the interaction of these promoting fire weather.

Surface temperature can directly affect fire risk because it controls the temperature of fuel. High temperatures mean the fuel is closer to its point of ignition, such that an approaching fire does not have to supply significant amounts of heat energy to start combustion (Schroeder and Buck 1970). A fire's rate of spread will therefore be greater in an environment characterised by high temperature.

Precipitation events can reduce the risk of ignition or suppress fires that are already burning. Water falling on the vegetation and on the soil increases a fuel's moisture content (FMC). Fuels characterised by high FMC require significant quantities of heat to accelerate evapotranspiration and ignite a fuel. Long periods of drought-like conditions can therefore give rise to intense fire seasons in which the frequency of fire, and the area burned by fire, are considerable.

1.3.3. Vegetation

Vegetation provides the fuel which fire burns, and is an important aspect of both the fire triangle and the fire environment triangle. Although vegetation in tropical and sub-tropical regions does not exhibit significant temporal variation, it does vary spatially. Vegetation cover types have different properties that in turn affect fire behaviour. These aspects include the fuel quantity and fuel size.

Fuel quantity is the amount of fuel available to burn. When a fuel is burned, it is the carbon that is combusted. Fuel quantity associated with a particular vegetation type can therefore be expressed as the amount of carbon per hectare (MgC/ha). Fire can burn with greater intensity, and release more heat, if there is more fuel to burn (Albini 1976).

Fuel size and shape determines the surface area to volume ratio of fuels. This varies significantly from forest stands and logs, to grasses and brush. Grasses and brush have high surface areas to volume ratios, meaning less heat is required to reduce moisture content and achieve the ignition temperature. Combustion in grasses and brush is further aided by a low fuel density. Conversely, dense fuels such as timber (forest) typically have low surface areas to volume ratios. This inhibits convective and radiant heat transfer, meaning that the time lag until ignition is achieved will be considerable. Combustion efficiency will also be limited within dense fuels as less oxygen is contained in fewer void/pore spaces.

1.3.4. Human influence

The human population can present both a risk to fire ignition, and are responsible for strict management strategies that controls fire behaviour and limits its frequency.

Ignition risk. Fire frequency has been found to be greater in close proximity to settlements, roads and agricultural land (Martinez *et al.* 2009). Roads can provide access to vulnerable fuels, which could be exploited by arsonists. Agricultural land poses a fire risk because fire is sometimes used by communities to clear fields. Grassland can also be a fire risk, as fire can occur here both naturally and as a form of management.

Topography influences the ability to **detect and respond** to fire. Finding the location of a fire can be difficult in terrain characterised by high relief that blocks the line of sight. Terrain also complicates the ability of communities to tackle fire. For example, on roads, travel time is relatively short compared to off-road movement through forest or on steep slopes.

The review of the fire environment above has highlighted numerous factors that could be incorporated into a fire risk model. These factors also fall into specific themes, from topography to weather to human influences. The following sections discuss how the influence of these factors can be incorporated into a model, with two different methods being critically compared.

1.4. Fire risk modelling approach

1.4.1. Limitations of existing methods

Over the past two to three decades, GIS has developed to become a major platform on which spatial decision making is performed, handling data at multiple spatial and temporal scales (Jiang and Eastman 2000). Multi-criteria evaluation (MCE) or multi-criteria decision analysis (MCDA) has been a central part of this development, enabling users to incorporate numerous (and often unrelated) aspects that affect a system or issue. By considering a wide variety of factors, decisions concerning suitability or vulnerability can be evaluated, producing reliable results that can be accepted by opposing interest groups.

1.4.2. Comparison of Boolean and fuzzy set standardisation

MCE has been used extensively within the fire research community, particularly studies concerning fire risk modelling and management (Vadrevu *et al.* 2010; Rathaur 2006; Orozco *et al*. 2009 ; Mohammed *et al.* 2009). As with the majority of MCE studies, factors that are deemed to contribute to or mitigate fire risk are identified. The factors (e.g. slope or aspect) can then be classified or standardised into a fire risk index. Areas that are considered 'vulnerable' are assigned a high index value (e.g. 10), while areas of decreasing vulnerability receive correspondingly lower values (e.g. 1). Standardising factors in this way is essential if factors are to be aggregated to produce an overall risk map.

This type of standardisation is Boolean in nature, in that discrete boundaries exist between index values. However, it is this Boolean-type standardisation that is a limitation of this method (Iliadis 2005). The equations below will be used to explain this limitation, and are based on the studies of Zadeh (1965), Burrough (1989) and Schubert (2004).

$$A = \{x | x \text{ has property } P\} \qquad x \in X \qquad \textbf{Equation 1}$$

Equation 1 means that all observations x within universe or population X with the property P are a member of class A. Applying this equation to a Boolean classification means that x either belongs to or does not belong to class A. Sharp crisp boundaries b and c therefore exist between occurrence (= 1) and non-occurrence (= 0) and could also be represented as shown in Equation 2 below. Boolean or classical set theory therefore satisfies two laws put forward by philosophers who devised the theory of logic, or 'Laws of Thought' (McBratney and Odeh 1997). The *law of excluded middle* states that every proposition is either true

or false (1 or 0), prohibiting any third possibility or membership (Robinson 2003). The *law of extended contradiction* states that a proposition cannot be both true and not true (e.g. a single location cannot exhibit characteristics of both categories).

$$\mu_A(x) = \begin{cases} 0 \text{ for } x \leq b \\ 1 \text{ for } b < x < c \\ 0 \text{ for } x \geq c \end{cases} \qquad x \in X \qquad \textbf{Equation 2}$$

Rarely in reality do such crisp boundaries exist between neighbouring index values. Uncertainty, imprecision and ambiguity are inevitable or inherent parts of natural systems (McBratney and Odeh 1997), and Boolean-based analyses can fail to capture this. This can introduce a degree of error into the model. To demonstrate this, Table 1 and Figure 1 below give an example of how slope could be classified into a risk index, with a greater fire risk value assigned to higher slope values. It is unrealistic, however, that a slope value of 29.9° has received a lower fire risk value than a slope value of 30°. This shows that even if an individual knows a significant amount about fire risk, it remains difficult to draw (or they are limited by) the boundaries that must be established between risk classes.

Table 1: Example of slope classification into fire risk. Table adapted from Orozco *et al.* (2009)

Slope angle (°)	Fire index value
0 - 2.9	1
3 - 14.9	2
15 - 29.9	3
30 - 90	4

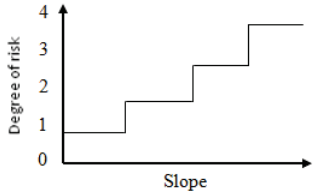

Figure 1: Sketch of Boolean method of slope classification.

Fuzzy systems are an alternative to the classical set theory described above (Zadeh 1965). Fuzzy modelling is designed to deal with phenomena where these boundaries are often vague, or where there is a gradual transition between fire risk classes (Robinson 2003). Fuzziness is therefore capable of incorporating the uncertainty that exists within the Boolean-type classification by introducing imprecision, and removing the need for sharply defined boundaries. However, by adopting a fuzzy approach, both the *law of excluded middle* and *law of extended contradiction* are violated because it allows a proposition to be true, false, or a partial membership of both. Figure 2 demonstrates how fuzzy set theory could be applied to the example of slope by applying a sigmoidal or S-shaped membership function to model the degree of risk. A membership function is in the form of an equation that is capable of mapping elements of a universe of discourse (e.g. raster cells in a slope layer) to their corresponding membership values (Yen 1999). Slope values below α are given

a minimal risk (0), while all slope values above γ are assumed to be at greatest risk (1). Between the two, a gradual change in membership is represented as a real number between 0 and 1. The sigmoidal membership function in figure 2 can be represented using Equation 3 from Robinson (2003):

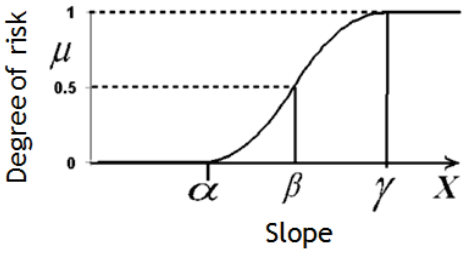

$$\mu = \frac{1}{1 + e^{-\beta(x-a)}}$$ **Equation 3**

Figure 2: A sigmoidal membership function that could be used to model fire risk. Adapted from Robinson (2003).

1.4.3. Boolean and fuzzy set operations

When the standardisation process discussed above has been completed, several overlapping layers exist, each with a degree of risk that varies both in magnitude, in space, and - in some cases - time. To produce a final vulnerability output capable of expressing this information, the layers must be aggregated or composited. Several operators exist which are capable of combining this information, including the AND, OR and NOT operators (Burrough 1989). The AND- and OR- operators for both Boolean and fuzzy sets will be critically discussed below.

Boolean AND-operator $A \cap B = \{x | x \in A \wedge x \in B\}$ **Equation 4**

The AND-operator considers only the intersection of 2 (or more) sets A and B. Equation 4 means that this intersection equals all objects x within the universe of objects X that are a member of sets A *and* B. The $\cap$ symbol signifies the use of intersection, and $\wedge$ denotes the use of the AND-operator.

Boolean OR-operator $A \cup B = \{x | x \in A \vee x \in B\}$ **Equation 5**

The union of sets A and B is performed by the OR-operator. Equation 5 above means that this union is equal to all objects x within the universe of objects X that are members to *either* A *or* B. The $\cup$ symbol signifies the use of union, and $\vee$ denotes the use of the OR-operator.

The problem that arises from aggregating layers that have been classified using Boolean logic lies not in the operators themselves, but in the arbitrary values assigned to each factor, and the discrete boundaries between these values (e.g. Figure 1). Any uncertainty or error that exists within each individual factor can be propagated and amplified when the operator is applied to it (Chen *et al.* 2010).

Fuzzy min-operator $A \cap B = \int_x \mu_A(x) \wedge \mu_B(x)/x$ **Equation 6**

The fuzzy min-operator is equivalent to the Boolean AND-operator, and was originally proposed by Zadeh (1965). The min-operator has also been referred to as a 't-norm' by Jiang and Eastman (2000). Equation 6 does essentially the same as Equation 4. However, the $\int_x$ symbol is used to show that the intersection is made on all objects x within the universe of objects X, and the / symbol represents 'with respect to'. Instead of denoting the use of the AND-operator, $\wedge$ represents the *minimum* of sets A and B.

Fuzzy max-operator $A \cup B = \int_x \mu_A(x) \vee \mu_B(x)/x$ **Equation 7**

The fuzzy max-operator is equivalent to the Boolean OR-operator, and was again proposed by Zadeh (1965). Jiang and Eastman (2000) refer to this operation as a 'co-norm'. Equation 7 is broadly similar to equation 5. The $\vee$ symbol represents the *maximum* of sets A and B.

The *laws of excluded middle* and *extended contradiction* are violated not only in the standardisation process, but also when the fuzzy min- max-operators are used. The *excluded middle* is violated because the final membership value that results from the operation is unlikely to be 'true or false' unless the inputs are themselves 1 or 0. The second law is broken because the operator integrates characteristics of two or more sets into one final value. For example, if the membership value of x in $A(x) = 0.5$, then $\bar{A}(x) = 0.5$. The intersection (or fuzzy-min) of A and $\bar{A}$ will therefore equal 0.5 ($A(x) \cap \bar{A}(x) = 0.5$) (Robinson 2003). The law of extended contradiction states that a proposition cannot be both true and not true, meaning the law is violated as the result is midway between 0 and 1.

Although the above operators have been used extensively within decision making science, the min- and max-operators do not allow the analyst to assert much control over how factors are combined. The min-operator will return only the lowest (minimum) value of the intersection whereas the max-operator returns the highest

(maximum) value of the union. These operators therefore reflect the worst and best case scenarios respectively (Robinson 2003). Jiang and Eastman (2000) refer to the min-operator as one that should be used within risk aversion, while the max-operator does the opposite, being optimistic by returning the highest value.

Convex combination was a method first employed by Charnpratheep *et al.* (1997). It is similar to the weighted combination technique applied in Boolean MCE, only that it is applied to fuzzy sets. The advantage of convex combination over the min- max-operators discussed above is that it gives the analyst control over how the fuzzy sets are aggregated. Weights can be applied to each individual fuzzy set to reflect its importance within the decision making process. For example, if slope was deemed to be of greater importance than aspect in its contribution to fire risk, a greater weight could be assigned to slope relative to aspect. The output between these two factors would therefore reflect the greater importance given to slope. The process of assigning weights to factors and summing is shown in Equation 8. In this equation $\mu_i(x_{ij})$ is the membership value of the j^{th} grid cell in a raster layer i, and w_i is the weight value assigned to layer i where $\sum_{i=1}^{m} = 1$ and $w_i > 0$.

Convex combination $F = \sum_{i=1}^{m} w_i \mu_i(x_{ij})$ **Equation 8**

The discussion of some frequently used operators has highlighted their main characteristics. The Boolean AND- and Boolean OR-operators provided the basis for the fuzzy MIN- and MAX-operators, which are used on fuzzy sets. However, these operators are limited in that the highest or lowest values are returned by the union or intersection of sets respectively. Convex combination, however, enables the analyst to prioritise, assigning weights to factors to represent their importance. This review will be used to formulate objectives in section 1.5.

1.4.4. Research problem

- MCE has been used extensively to assess suitability, vulnerability and risk.
- Factors important to the evaluation must first be standardised, then aggregated to produce final risk maps.
- **Boolean** method of standardisation creates **discrete and unrealistic** boundaries
- **Fuzzy** approach enables a **gradual transition** from high to low risk to be modelled, removing the need to introduce unrealistic boundaries.
- Standardised factors must then be **aggregated** using the **fuzzy MIN-** or **fuzzy MAX-operators**, or **convex combination.**

- Fuzzy MIN-operator returns the **minimum** of inputs, while fuzzy MAX returns the **maximum** of inputs.
- Convex combination enables the **importance between factors be expressed** by assigning weights.

1.5. Research objectives

Sections 1.3 and 1.4 focussed on two main areas, namely factors that influence fire risk, and a discussion of why a fuzzy approach to MCE has advantages over its Boolean counterpart. To visualise how these components can be brought together, a conceptual diagram was formed (Figure 3), and objectives to guide the study were developed. These objectives and research questions, stated below, also appear within the diagram to demonstrate how they will be achieved.

1. To locate burn scars within the study area.
- Can these burn scars be located on an ASTER image of the region?
- What other data sets exist from which burn scar information can be obtained?
- How are the burn scars distributed with respect to the selected fire risk factors?

2. To develop a spatial, dynamic fire risk model based on fuzzy logic.
- Which values can be found on which to base fuzzy membership functions?
- Which fuzzy membership functions are most suitable to fit to which parameters?

3. To validate the fire risk model based on fire scars within the study area.
- To what extent do the regions of high fire risk correspond with the burn scars?

4. To perform a sensitivity analysis on each sub-model weight
- How does the distribution and value of risk change as each sub-model's weight is varied?

These objectives will be applied to a study area in southern Nepal. The next chapter introduces this study area, describing details such as location, topography, climate and population.

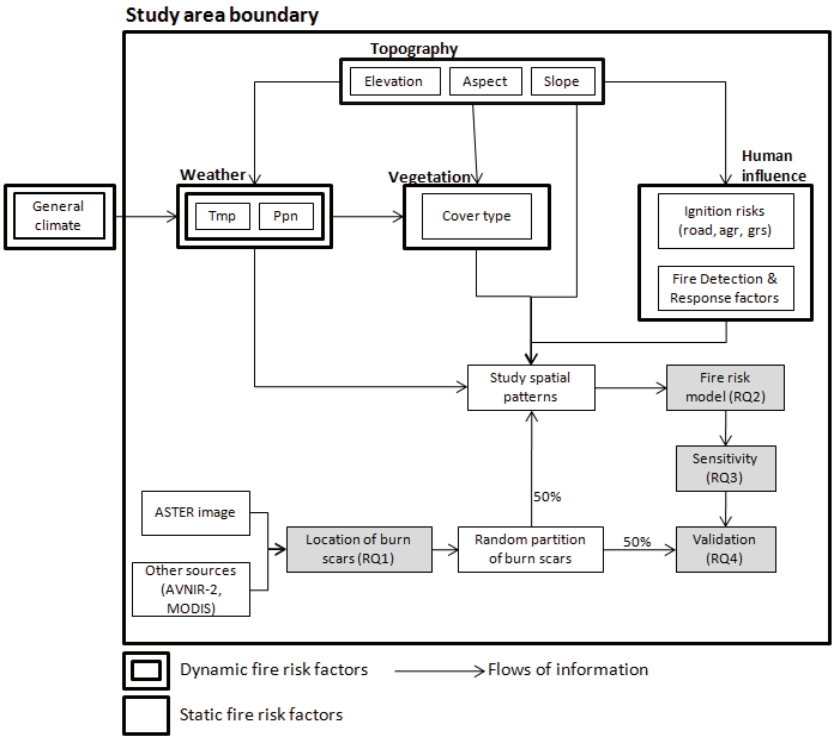

Figure 3: Conceptual diagram linking elements of a system that will form the basis of a fire risk model.

2. STUDY AREA

2.1. Location

The limits of the study area are based on an ASTER image from February 2008, with the exact corner coordinates of: 84.35°, 27.99° NW; 84.95°, 27.90° NE; 84.81°, 27.36° SE; 84.21°, 27.45° SW. The study area is centred around the district of Chitwan, located in south-central Nepal, with the districts of Nawalparasi, Tanahu, Gorkha, Dhading, Makwanpur and Parsa partially included (Figure 4). An area of 3754 km^2 is bounded by these coordinates.

This ASTER scene was chosen because *a)* it covers an area with a history of the fire issue and was also obtained during the fire season, *b)* the scene is also characterised by varying terrain, and *c)* the scene is characterised by a low degree of cloud cover.

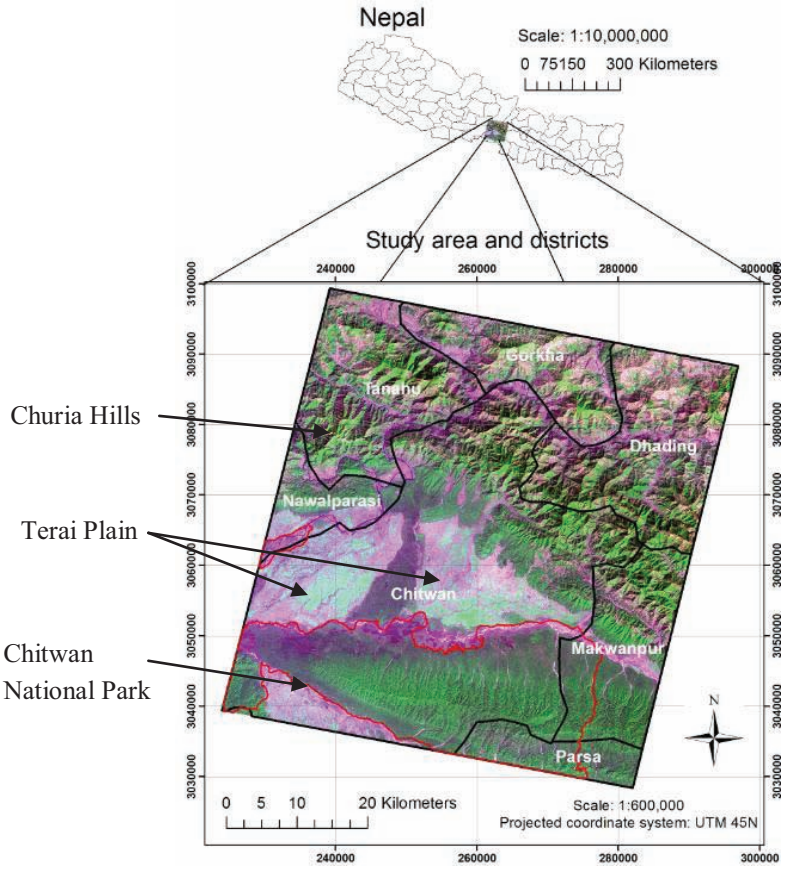

Figure 4: Study area

2.2. Topography

The study area is characterised by different landscapes that vary along a north-south direction. The Churia Hills are steep mountains (>45°) found in the north of the study area, with elevation reaching over 2,000 m. These mountains are not as high as the ranges further north, but this means fire occurrence is still experienced. The mountains give way to a largely flat plain (Terai plain) located in the centre of the image, with elevation here typically 170 m. The southern portion of the image is occupied by Chitwan National Park and Parsa Wildlife Reserve. Established in 1973, the park encompasses a long, continuous ridge running in the east-west direction, with elevation reaching over 700 m. The area is highly biodiverse with 700 species of wildlife. Of this number, 540 are birds, such as kingfishers, storks and eagles. There are also several species of reptile including the king cobra, the Indian starred tortoise, monitor lizards, and mugger crocodiles. However, Chitwan National Park is perhaps most famous for its mammalian wildlife such as the Bengal tiger, Indian rhino and Asian elephant. Continuing further south from the park, one would cross the border into India. However, this is not included in the ASTER image.

2.3. Climate

A sub-tropical climate characterises this study area, even within the hilly region in the north of the study area. Dry and wet seasons therefore dominate, with monsoon rains falling between June and mid-September every year, while the driest months are those of March, April and May which is traditionally the fire season (Figure 5). Temperatures are highest prior to the onset of the monsoon season, approaching 40° C. Lowest temperatures are experienced in December/January, but begin to increase from February.

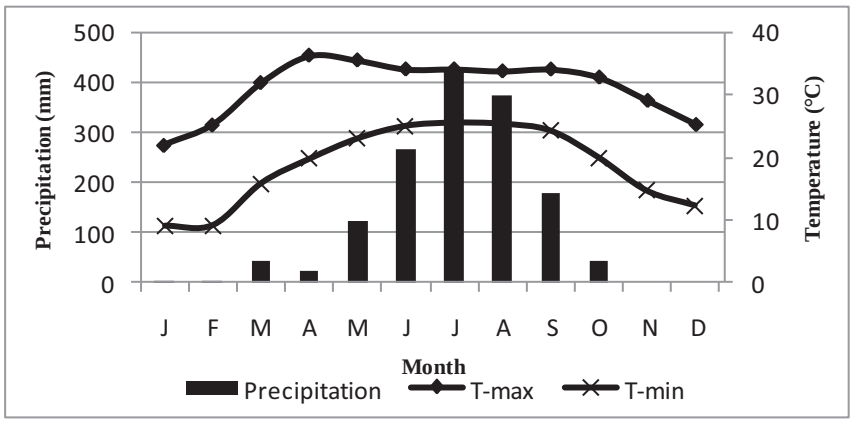

Figure 5: Average max/min temperature and total precipitation for Bharatpur airport, Chitwan, 2008.

2.4. Land cover and Land use

2.4.1. Forest cover

A significant proportion of the study area is covered by sub-tropical deciduous forest. Sal (*Shorea robusta*) is the most common tree species, for example comprising up to 70% of tree species within Chitwan National Park. Other species include Asna, Chilaune, Kyamun and Valayo. The soil on which these species grow is predominantly alluvial with a high clay content, and found throughout the Terai region and Churia Hills. The nutrient content is described by the FAO as fair to medium, although the oldest soils are poor (FAO 1998). When mature, sal trees can rise up to 40 m in height, with diameter at breast height exceeding 120 cm. These hardwood species are fire resistant, and can withstand the majority of wildfires. However, other tree species, or those not mature, have lower resistance to fire, and therefore can be destroyed.

Depending on the proximity of the forest to human settlements/activities, the forest also exhibits different densities. Low density forest is typically located closest to settlements, while forest at higher elevation, and at greater distances are less disturbed. Compared to low density forest, dense forests are characterised by a greater number of trees that are generally more mature. Dense forest also has a high quantity of shrubs and small trees that can reach up to two to three metres in height.

2.4.2. Agricultural land

Most agricultural land is situated on the plain in the centre of the study area. This region is important for Nepal in that favourable growing conditions, combined with the flat land ensures that a significant amount of food can be grown to support communities in the foothills and mountains to the north, where suitable ground is limited. The major crop grown is rice, although pulses and other vegetables are also grown. Rice is harvested in October/November. In March, fields are deliberately burned to clear the land, and to promote the growth of the next crop. In the mountains, subsistence agriculture supports the communities situated here. Rice is again the most important crop, and is grown on terraces on the steep hill sides. There are few farms devoted specifically to livestock as most households have their own animals such as chickens, goats and cattle.

2.4.3. Grassland

Grasslands are located along the northern edge of Chitwan National Park, where elevation is low and the land flat. Height of these grasslands approaches 4 m, and is an important habitat for deer. Fires within these grasslands are frequent. Some of the fires are natural, but some fires are prescribed for management purposes. For example, some deer species rely on the shoots that germinate from the burned grassland.

2.5. Population

Chitwan is the largest district situated within the study area, and has a population of approximately 470,000, the majority of which are either Hindu or Buddhist. Of this number, 225,000 inhabitants live within Narayangadh/Bharatpur, the largest city within the province. This city is also a major commercial hub within southern Nepal, and one of the country's fastest growing urban centres. In the past, agriculture was the city's main source of income. More recently, however, there has been a shift towards other industries, with large multinationals such as Coca-Cola and San Miguel arriving. Other industries include the poultry industry, which supplies domestic markets and exports to India.

The majority of the remaining inhabitants live within agricultural communities on the Terai Plain. The Churia Hills to the north are occupied by an ethnic minority group called the Chepang. This tribal group used to be nomadic, but more recently have settled into isolated and inaccessible communities that rely on subsistence farming. The Chepang language is one of the few to use a duodecimal (12 base) counting system.

3. METHOD

A review of fire related literature in chapter 1 was an important step in the selection of fire risk factors to be used in the development of a fire risk model. These factors were assigned to groups sharing similar characteristics, and related to the research objectives shown in the conceptual framework (Figure 3). It was then possible to start acquiring the data which would eventually form model components.

3.1. Data acquisition

3.1.1. Pre-fieldwork

A 30 m DEM obtained from the ASTER14DEM product, was used to derive aspect and slope maps. Two of the most recent ASTER scenes for the study area were downloaded from USGS via the GLOVIS viewer. These were imported into ERDAS IMAGINE and georeferenced using the attached metadata file. The dates of the two ASTER scenes were 21/02/2008, and 24/03/2008. For more discussion concerning these layers, including information on the sources, limitations and justification of use, see Appendix 1. An unsupervised classification of the study area was also performed for use in fieldwork.

3.1.2. Fieldwork

Time was spent at the International Centre for Integrated Mountain Development (ICIMOD) headquarters in Kathmandu to gain more information about the study area, possible sources of data, and receive advice. A major source of data acquired was an ALOS AVNIR-2 burned area dataset from March 2010. ICIMOD also recommended the use of TRMM and MODIS/Terra data for rainfall and temperature as the study area was limited by few climate stations. For more information on these datasets, see table 18 in the appendix. Unfortunately, no (relevant) wind data was available from the climate stations in the area - data ceased to be recorded from 1998. A search was performed to find alternative sources of wind data, such as satellite estimated data, but nothing suitable was found. It was therefore not possible to include wind data within this study.

Fieldwork was conducted in the study area between the 24th September and 13th October 2010. The most important task within this period was to locate burn scars. This involved navigating to MODIS detected ignition points using an IPAQ and, where possible, digitising the scar boundaries. The IPAQ was also used to navigate to the burned area locations within the AVNIR-2 dataset. To provide an assessment of accuracy of this dataset, GPS measurements were recorded, stating whether scar

evidence existed or not at that location. Burn scars were also digitised from an ASTER scene of March 2008, using the 231 band composite that has been proven to be effective in identification of burn scars (Orozco *et al*. 2009). These scars were only digitised in the northern 40% of the study area because the ALOS AVNIR-2 dataset did not extend to this region. It was not possible to provide an accuracy assessment of the ASTER burn scars because they dated to 2008, and so would have been re-colonised by vegetation. Furthermore, access to the northern part of the study area was limited due to difficult terrain found here, so it was not possible to navigate to ignition points. This justified the digitising of burn scars from 2008.

Approximately 190 ground truth points were collected for assistance in classifying a land cover map. Points were collected randomly in the Terai Plain, in grassland along the northern boundary of Chitwan national park, and in the Kayar Khola watershed. However, in the northern part of the study area in which the Churia Hills dominate, points were not collected randomly due to a high degree of inaccessibility. In such situations, points were taken close to roads. The categories recorded consisted of: Agricultural land, urban, grassland, low density (or degraded) forest, and high density forest.

The road network within the study area was digitised using an IPAQ. Roads that were not visited during fieldwork were digitised from the ASTER image. The ASTER image was used because the roads were sufficiently visible, and was more up to date than the road maps (2008 vs. 1990s).

3.2. Data preparation and pre-modelling phase

3.2.1. Image classification and accuracy assessment

190 GCPs were collected during fieldwork. These were used to perform a supervised maximum likelihood classification on agriculture, grassland, low density forest and high density forest. Urban areas and the rivers were digitised because *a)* the two were not well classified in early attempts, and *b)* these land cover types had distinct enough boundaries that were easily digitised. 50% of the GCPs were (randomly selected) for training, while the remaining 50% were used for validation. The overall accuracy of the land cover classification (for four classes) was 82%, with a kappa coefficient of 0.75. An accuracy assessment was also performed on the AVNIR-2 burned area dataset of the study area. The overall accuracy was 89%, with a kappa coefficient of 0.73. For full results, see Appendix 2, 3, 4 and 5.

3.2.2. Random partition of burn scars

790 burn scars were identified within the study area. In order to develop the fire risk model and perform the validation exercise (research objectives 2 and 3), it was necessary to develop a method to randomly select burn scars within the study area. Random, non repeating integers between 1 and 790 were generated, and these were then matched to the unique IDs of the burn scars. The selected burn scars were then checked to ensure an even distribution across the study area, and to ensure that the total area between calibration and validation scars was similar. This resulted in 395 burn scars to calibrate the model with, and 395 to perform a validation.

3.2.3. Overlaying calibration burn scars with factor maps

Exploring the spatial patterns of the burn scars is essential because it provides information about where significant numbers of fires have (and have not) occurred, and whether there is any pattern at all. To explore these patterns, overlays were performed with a number of the factor maps (see Figure 6). The value extracted from a single burn scar represented the mean value of all cells that are enclosed by the boundary of that scar. The data was exported to a spreadsheet, and histograms were created.

A subjective element that arises when using histograms is that their shape can change depending on the number and size of bins. To mitigate this effect, a sensitivity analysis was performed on each risk factor's histogram. This process involved systematically increasing the number of bins, starting with a few bins to many bins. To view the results of this sensitivity analysis, see the Appendix 6.

Another important factor to consider when using histograms is to account for the area of land contained within each bin range, as this is unlikely to be equal between bins. This in turn affects the reliability of the histogram. For example, if a bin has a low number of fire scars, it may simply be because the total area of land occupied by that bin is also small. To overcome this problem, the number of scars located within a bin was divided by the total area occupied by that bin to derive scars per ha.

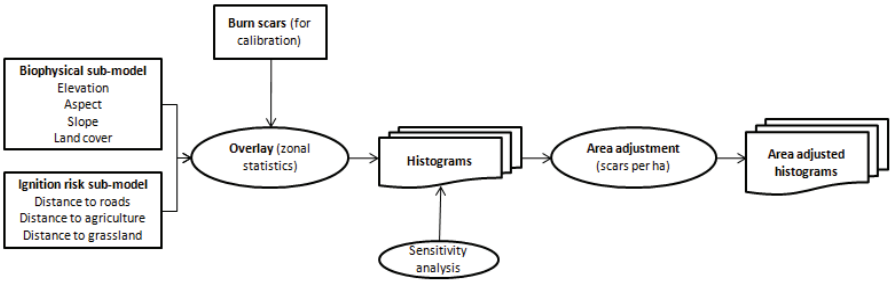

Figure 6: Flow diagram summarising steps taken to extract information about the spatial patterns of burn scars.

3.3. Modelling phase

3.3.1. Overall model structure

The development of a fire risk model will be based on those developed by Rathaur (2006) and Orozco *et al.* (2009). This approach identifies individual fire risk factors, and groups them into sub-models which share similar characteristics. Five sub-models have been included which aim to encompass the range of aspects that give rise to 'fire risk' (Figure 7). These are the biophysical risk, weather risk, ignition risk, fire detection and fire response sub-models. A final fire risk output is produced by combining these sub-models by use of a weighted combination as used in Rathaur (2006). It is also possible to add a dynamic aspect to the fire risk model by providing updated climate parameters over time, as performed by Orozco *et al*. (2009).

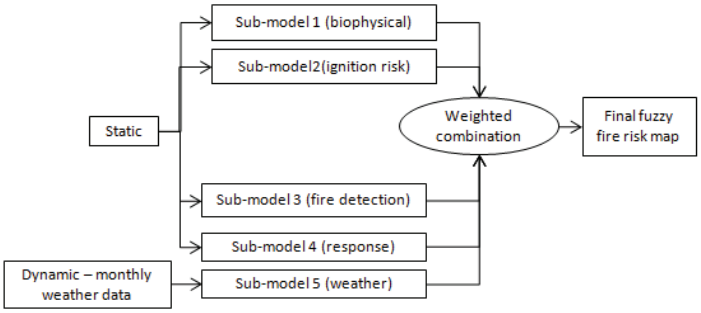

Figure 7: Fire risk model structure

3.3.2. Biophysical sub-model

The biophysical sub-model consists of elevation, aspect, slope and land cover. As discussed in chapter 1, these topographical and vegetation factors interact to

influence the location at which a fire is likely to occur. Figure 8 below indicates the steps taken to integrate these factors and develop the first sub-model.

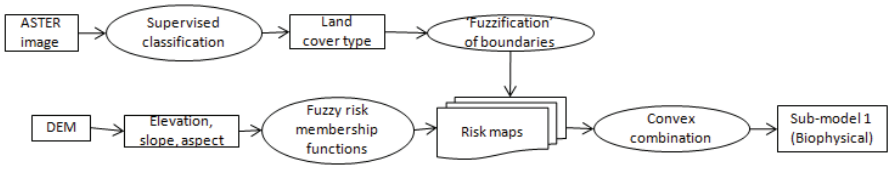

Figure 8: Biophysical sub-model

The histograms developed by overlaying the calibration burn scars with the factor maps provided information on their spatial patterns. The histograms were then used as a base onto which fuzzy risk membership functions were applied. Single equations were used to model the degree of risk. Generally, the histogram category which had the greatest number of scars per ha was assumed to have the greatest fire risk. All cells contained within the highest risk bin were assigned a value of 1.0 by use of the equation, with decreasing values representing lower degrees of risk. Equations were chosen based on how well they approximated the shape of a histogram.

Application of fuzzy membership functions to biophysical risk sub-model

Elevation

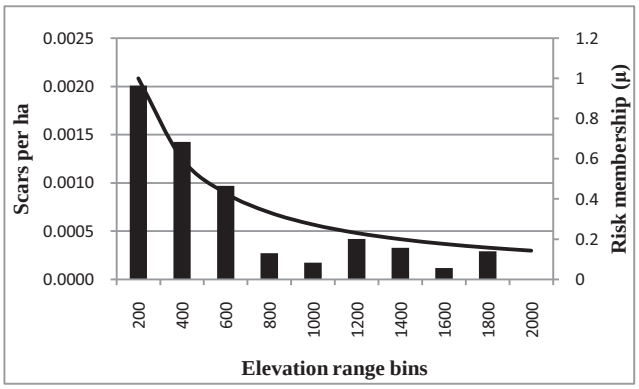

$$\mu = \frac{1}{1 + \left(\frac{x - \beta}{\delta}\right)}$$

Equation 9a

$$\mu = \frac{1}{1 + \left(\frac{x - 200}{300}\right)}$$

Equation 9b

Figure 9: Elevation histogram and membership function.

A decreasing exponential function (generalised bell function) was applied to the elevation histogram (figure 9) using equation 9b above, adapted from Robinson (2003). ß is the value at which risk membership is greatest (1), while δ controls the

rate at which μ(x) approaches 1 (Schubert 2004). All values of elevation less than 200 m were assigned a value of 1.

Aspect

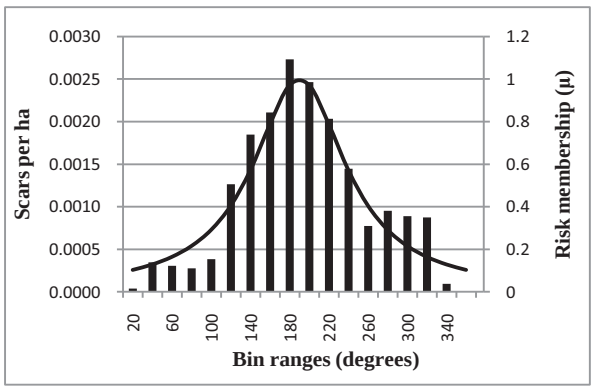

$$\mu = \frac{1}{1 + \alpha(x - c)^2}$$

Equation 10a

$$\mu = \frac{1}{1 + 0.0003(x - 170)^2}$$

Equation 10b

Figure 10: Aspect histogram and membership function.

A Gaussian function was applied to the aspect layer as the shape approximated by the histogram (figure 10) was a normal distribution. Equation 10b above was applied, where c denotes the 'central concept' where risk is greatest, and α represents the rate at which μ(x) approaches 1 (Schubert 2004).

Slope

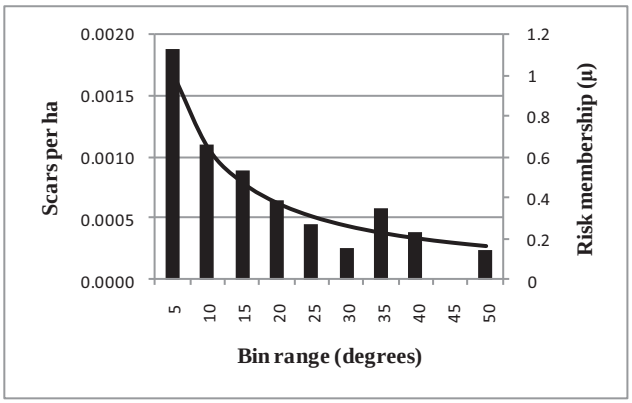

$$\mu = \frac{1}{1 + \left(\frac{x - \beta}{\delta}\right)}$$

Equation 11a

$$\mu = \frac{1}{1 + \left(\frac{x - 5}{9}\right)}$$

Equation 11b

Figure 11: Slope histogram and membership function.

Similar to elevation, a decreasing exponential function (generalised bell function) was applied to the slope histogram (figure 11) using equation 11b above, adapted from Robinson (2003). All slope values less than 5° were assigned a value of 1.

Land cover

Land cover is a significant element of the fire risk model because it provides information on the fuel characteristics of the study area. If no fuel is present, no ignition can occur, even if the area in question is high risk with respect to elevation, slope and aspect.

The calibration burn scars were overlaid with the classified land cover map to extract information regarding fire occurrence. The initial risk values assigned to the land cover types was based on the scars per ha (Figures 12). The land cover type with the greatest number of scars per ha was assigned the highest risk. These initial risk values are Boolean, in that the risk assigned was uniform across each land cover type (Table 2).

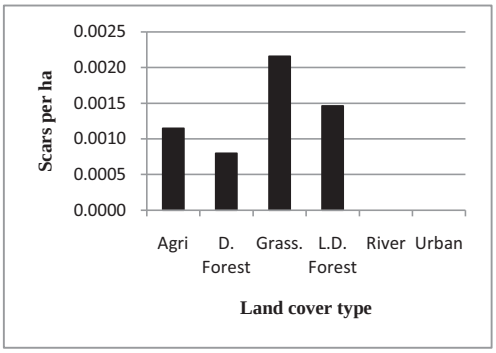

Table 2: Initial Boolean risk membership values.

Land cover	Risk
Grassland	1.0
Low density forest	0.8
Agriculture	0.6
Dense forest	0.4
River	0
Urban	0

Figure 12: Land cover histogram using burned area per ha

'Fuzzification' of land cover boundaries and application to risk membership

Although the land cover map used in this study was classified with 82% overall accuracy (kappa = 0.75), the map shows that sharp boundaries exist between land cover types. In reality, these boundaries can be vague, with a gradual continuum from one land cover type into another (Lu and Weng 2007). Methods employed to

overcome this problem include the use of soft classifiers, such as fuzzy c-means, whereby each pixel to be classified is assigned a membership to a particular land cover type. However, a limitation of soft classifiers such as fuzzy c-means is that it can introduce accuracy assessment issues (Silván-Cárdenas and Wang 2008).

Within the soil science discipline, the use of soil maps has created issues similar to those within land cover mapping in that discrete boundaries exist between soil units. However, Lagacherie *et al.* (1996) proposed the use of transition zones that lie across these soil boundaries, accounting for the gradual continuum between soil units. Within a transition zone, a fuzzy membership function is used to assign a pixel a degree of membership to the soil unit it is located within. Regions of a soil unit that are not located within the transition zone are assumed to have full membership to that soil unit, so this method assumes that the fuzziness only lies within the transition zone, and not outside it.

This same approach was applied to deal with the discrete boundaries between land cover types (Figure 13). A subjective element of this method is choosing the width of the transition zone around the boundary. During fieldwork, it was noticed that in several locations, a transition zone of approximately 500 m existed between cover types, especially in the region adjacent to Chitwan National Park. To model this transition zone within a GIS environment, a Euclidean distance function with a maximum extent of 250 m was performed on the boundaries between land cover types (250 m each side of the boundary). Linear membership functions (Equation 12) were then applied to each land cover type to model the degree of membership.

An intersect function was then used on each land cover type to isolate other land cover transition zones which overlapped onto it (e.g. for the transition zone of agriculture, intersect was used to isolate overlapping zones of grassland, low density forest and dense forest etc.). The overlapping regions for each land cover type were then combined using equal weights. However, the magnitude of each weight differed depending on how many land cover transition zones were overlapping at a given location (e.g. in some areas, only two land cover types overlapped, such as agriculture and grassland, but in other cases, three or four land cover types were overlapping).

The fuzzy land cover boundaries were then used to adjust the risk values associated with each land cover type assigned in Table 2. This was achieved by multiplying the fuzzy land cover boundaries with the risk map. This had the effect of reducing the

level of risk associated with land cover types at the boundaries, as the confidence with which a pixel belonged to a land cover type was also less.

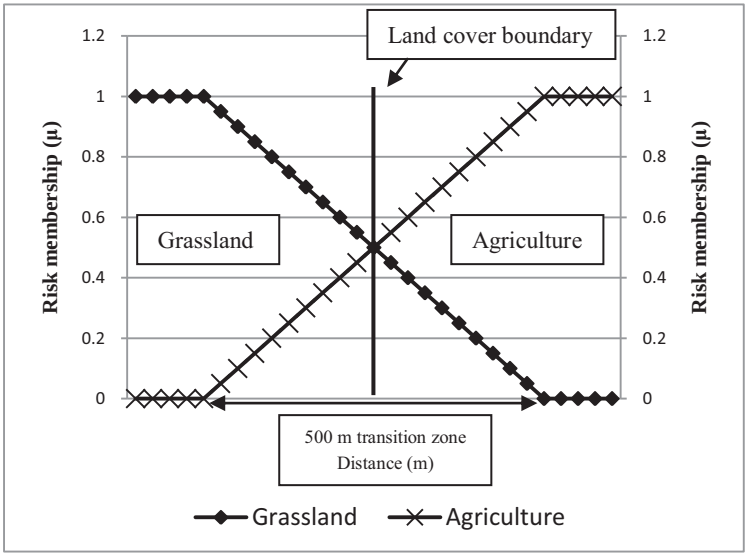

$$\mu = \frac{\beta - x}{\beta - \alpha}$$

Equation 12

Figure 13: Example of fuzzy transition zone

3.3.3. Ignition risk sub-model

Euclidean distance functions were performed on the road network, agricultural and grassland layers to derive proximity surfaces. The calibration burn scars were then overlaid onto these surfaces to provide the data on which the histograms below are based. It is important to note that the distance function does not include scars situated within the land cover type (i.e. 0 km), but does include all scars that are located 0.1 km or more from that cover type. Figure 14 indicates the steps taken to develop the second sub-model.

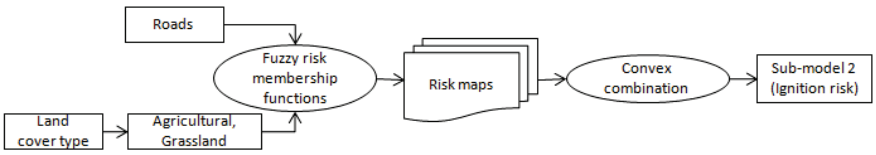

Figure 14: Ignition risk sub-model

Application of fuzzy membership functions to ignition risk sub-model

Distance from roads

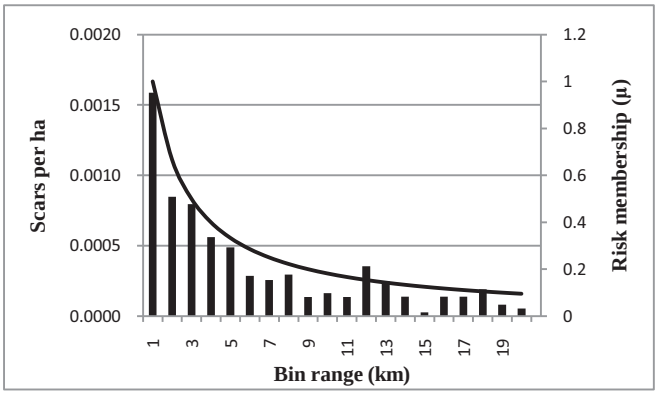

$$\mu = \frac{1}{1 + \left(\frac{x - \beta}{\delta}\right)}$$

Equation 13a

$$\mu = \frac{1}{1 + \left(\frac{x - 1}{2}\right)}$$

Equation 13b

Figure 15: Distance from roads histogram and membership function

A decreasing exponential function was applied to the distance from roads layer (Figure 15), using equation 13b above (Robinson 2003). A value of 1 was assigned to all distance values between 0.1 and 1 km from roads.

Distance from grassland

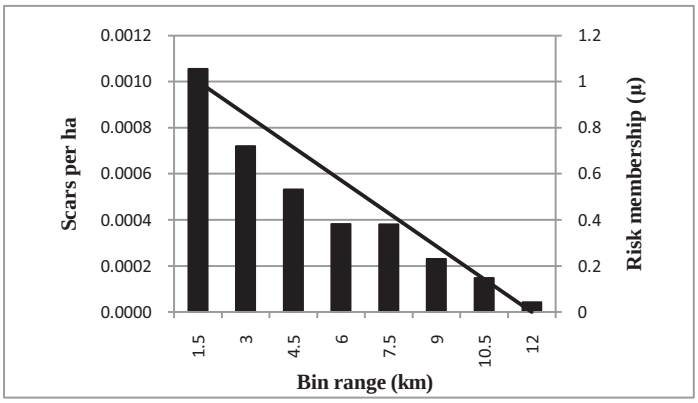

$$\mu = \frac{\beta - x}{\beta - \alpha}$$

Equation 14a

$$\mu = \frac{12 - x}{12 - 1.5}$$

Equation 14b

Figure 16: Distance from grassland histogram and membership function

A decreasing left trapezoidal function was applied to the grassland histogram (Figure 16), using equation 14b adapted from Robinson (2003). ß is the value at

which risk membership becomes 0, while α is the value for maximum risk. Values less than 1.5 km from grassland were assigned a value of 1.

Distance from agriculture

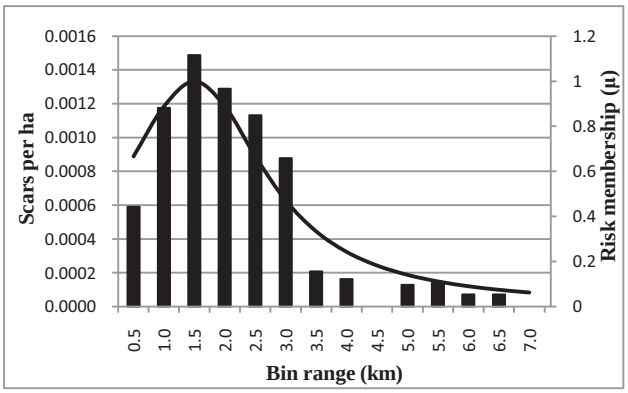

$$\mu = \frac{1}{1 + a(x - c)^2}$$

Equation 15a

$$\mu = \frac{1}{1 + 0.5(x - 1.5)^2}$$

Equation 15b

Figure 17: Distance from agriculture histogram and membership function

A skewed Gaussian function was applied to the distance from agriculture (Figure 17), with a central concept of 1.5 km (Equation 15b). A limitation of this function, however, is that it overestimates the risk land between 0.1 and 0.5 km from agriculture.

3.3.4. Weather sub-model

Prior to fieldwork, the intention was to incorporate wind and relative humidity data into the fire risk model. However, this was not possible due to a lack of data. Precipitation and temperature data alone are therefore relied on to assess fire risk with regard to the weather sub-model. Generally, low precipitation and high temperatures promote fire risk. Figure 18 depicts how precipitation and temperature were used to develop the weather sub-model.

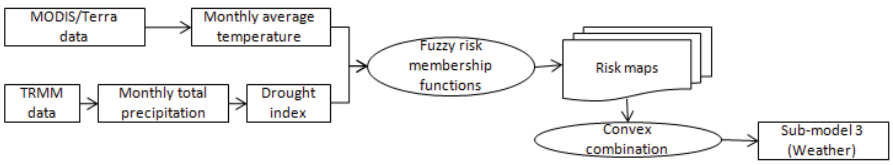

Figure 18: Weather sub-model

Precipitation

Precipitation directly affects a fuel's moisture content, and therefore the likelihood of a fire igniting and propagating (Chuvieco *et al.* 2004). However, the risk of this occurring is not only affected by current rainfall conditions, but also by the conditions that characterise the previous months. It is therefore important to consider not only the magnitude of rain received, but also when that rain was received. Drought indices are capable of expressing these two different dimensions. To account for this, we look for an index capable of expressing these two different dimensions. The China Z-Index (CZI) is one such suitable index.

China Z-index

The CZI is a drought index used by the National Climate Centre of China (NCC), and was first introduced in the 1990s. The CZI produces similar results to the Standardised Precipitation Index (SPI), a commonly used drought index developed in the US by McKee *et al.* (1993). The two both express the degree of dryness or wetness as a z-score between approximately -3.0 (extreme drought) to +3.0 (extreme wetness). The CZI has been found to follow the SPI closely, producing similar index values, although in severe droughts the CZI can overestimate the dryness (Wu *et al.* 2001; Morid *et al.* 2006). An advantage of the CZI and SPI is that only monthly precipitation data is required to assess the degree of drought, and both can be adapted to 1-, 3-, 6-, 9-, and 12-month time scales depending on the aim of the research. For example, a 3-month timescale can be useful for monitoring agricultural drought, while hydrologists may use a long-term, 12-month timescale. The CZI is used in this study, however, because it is relatively simple to calculate compared to the SPI. Furthermore, some authors (e.g. McKee *et al.* 1993) recommend a minimum of 30 years data to achieve reliable results for the SPI, while only 13 years of data is available in this study.

The CZI assumes that the precipitation data obeys the Pearson Type III distribution (Guttman 1999). The equations below show how the CZI is calculated and are from Wu *et al.* (2001):

$$Z_{ij} = \frac{6}{C_{si}} \left(\frac{C_{si}}{2} \varphi_{ij} + 1 \right)^{1/3} - \frac{6}{C_{si}} + \frac{C_{si}}{6} \qquad \textbf{Equation 16}$$

Where Z_{ij} is the CZI, i is the timescale of interest (1-, 3-, 6-months etc.), and j is the current month (equation 16),

$$C_{si} = \frac{\sum_{j=1}^{n}(x_{ij} - \bar{x}_i)^3}{n * \sigma_3{}^3}$$ **Equation 17**

where C_{si} is the coefficient of skewness and n is the total number of months in the record (equation 17),

$$\varphi_{ij} = \frac{x_{ij} - \bar{x}_i}{\sigma_i}$$ **Equation 18**

where φ_{ij} is the standardised variate (Z-score), x_{ij} is the precipitation of month j for period i, $\bar{x}_i$ is the mean for period i, and σ_i is the standard deviation of period i (equation 18). For this study, CZI values were calculated for the 3-month timescale. As mentioned above, a 3-month timescale is useful when studying agricultural drought because this is an approximate timescale over which soil moisture responds to (a lack of) precipitation (McKee *et al.* 1993). In this study, it will be assumed that low soil moisture corresponds to low vegetation moisture, which should be reflected by negative CZI values. Negative CZI values are therefore associated with greater fire risk.

Calculation of CZI using TRMM data

Figure 19 below depicts the steps taken to calculate the CZI using TRMM monthly total precipitation data, and how this CZI was visualised within a GIS environment.

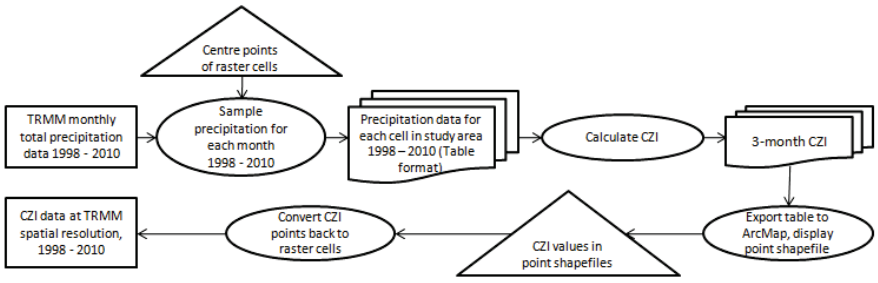

Figure 19: Calculation of CZI

Application of fuzzy membership function to CZI

The average CZI value was calculated for each month in the 1998-2010 period. As this model was run for only 12 months, the CZI values between September 2009 and August 2010 were plotted in Figure 20 below. Equation 19b was used to model the degree of risk. A CZI value of 2.024 was chosen as the central concept on which this equation was based. This value was the highest CZI value calculated throughout the 1998-2010 period, and was chosen so that all calculated risk values would compare to this. This means the same equation could also be applied to the monthly CZI for any time period between 1998 - 2010.

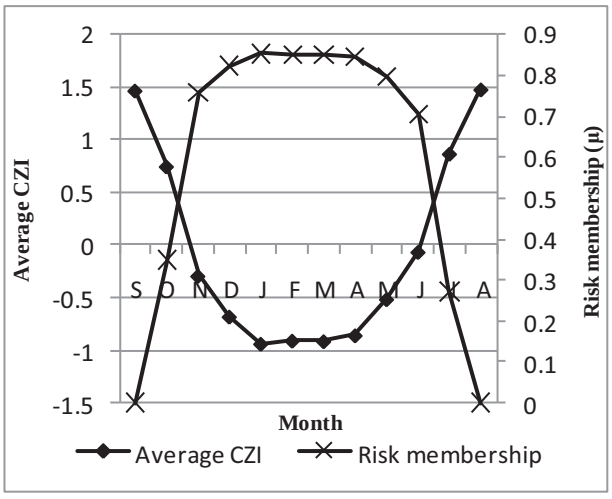

$$\mu = 1 - \left(\frac{1}{1 + a(x - c)^2}\right)$$

Equation 19a

$$\mu = 1 - \left(\frac{1}{1 + 1(x - 2.024)^2}\right)$$

Equation 19b

Figure 20: Average monthly CZI values and corresponding risk membership

Temperature

High temperatures can increase fire risk due to the effect on evapo-transpiration, and the reduction of fuel moisture content (Chuvieco *et al.* 2004). Months characterised by greater temperatures are therefore associated with increased fire risk as the litter layer and deadwood are dried, and live vegetation is stressed.

Rather than using raw temperature (°C) data alone to model the degree of risk, Z-scores were calculated for each month for which data was available (January 2000 to August 2010), and it was assumed the data was normally distributed. To calculate

the Z-scores and visualise them within a GIS environment, a similar method was followed as depicted in Figure 14. The calculation of Z-scores for this period is useful because it presents the temperature of a month as its standard deviation from the mean, providing an insight into how warm or cold it is compared to other months.

Application of fuzzy membership function to temperature

Similar to the CZI values, the average Z-scores were calculated for each month between the 2000 - 2010 period. The Z-scores for the 12 months in which the model was run are presented in Figure 21. Equation 20b was used to model the risk associated with each month. The value chosen as the central concept *c* was 2.44, the highest Z-score value for the 2000 - 2010 period. This was chosen so that all calculated risk values would compare to this.

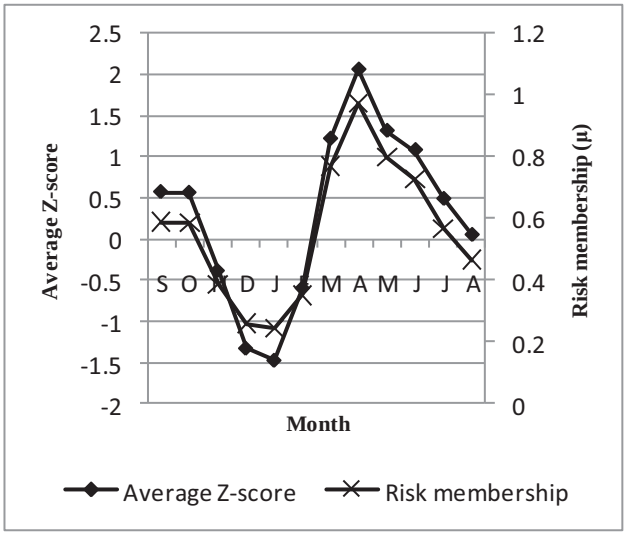

$$\mu = 1 - \left(\frac{1}{1 + a(x - c)^2}\right)$$

Equation 20a

$$\mu = 1 - \left(\frac{1}{1 + 0.2(x - 2.44)^2}\right)$$

Equation 20b

Figure 21: Average monthly Z-score values and corresponding risk membership

3.3.5. Detection sub-model

Fires must be detected before measures can be taken to limit the damage caused, promoting the importance of a detection sub-model (Figure 22). A viewshed analysis is capable of modelling this detection aspect, identifying all cells in a raster input (usually a DEM or digital terrain model (DTM)) that are visible from designated observation points or view lines (ArcGIS 10 Help 2010). The viewshed function scans in the azimuthal (horizontal) and vertical plains, identifying regions of a raster input which breaks or limits the scan. The user is also able to specify a radius, beyond which nothing is visible.

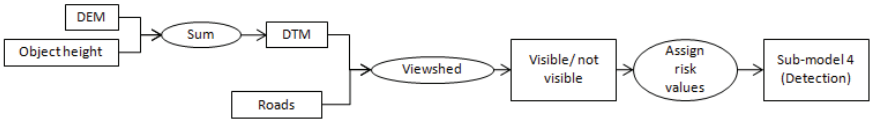

Figure 22: Detection sub-model

As the road network for this study area passes through all major settlements, as well as rural communities, it was decided that a viewshed analysis conducted only from the road network was adequate to provide comprehensive coverage. The Geospatial Modelling Environment was used to create points every 2 km along the road network. These locations were used as observation points for the viewshed. A DTM was created by adding the approximate height of the land cover types on to the DEM. Viewer height was set at 1.8 m to approximate the height of a person.

It is not possible to apply fuzzy membership functions to the viewshed analysis, as areas can only be simply visible or not visible. In this situation, a Boolean type approach must be adopted to reflect the degree of fire risk. Regions which have been identified as not visible from a road network are a greater fire risk because it will take longer to discover if a fire has ignited, while the opposite is true for areas that are visible. Table 3 below presents the risk values to be assigned to the visible/not visible categories, and is based on values assigned by Orozco *et al*. (2009).

Table 3: Detection risk sub-model

Detection category	Fire risk value
Visible	0.9
Not visible	0.2

3.3.6. Response sub-model

When a sufficiently large fire has been detected, actions should be taken to limit the damage it can cause. The length of time between detecting the fire and bringing it under control is known as the response time. However, this response time is affected by the terrain through which foresters and concerned communities must travel to reach the fire, and includes factors such as slope, elevation and land cover. Travel along roads is also significantly shorter than travel off road.

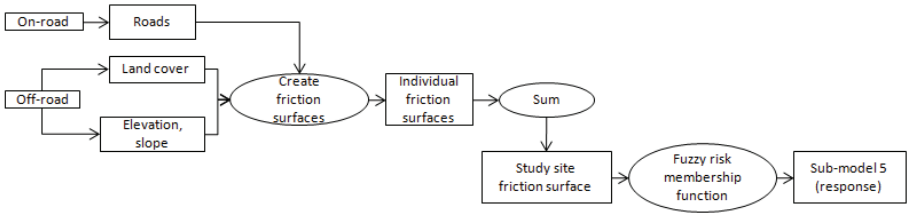

Figure 23: Response sub-model

Friction surfaces were created by reclassifying factor maps into values that reflect the difficulty individuals would face in moving through terrain (Figure 23). The values that have been assigned to these factor maps are presented in tables 4 to 6 below, and are based on the values used by Orozco *et al.* (2009). A cost-distance function was then applied to these factor map based on the assumption that response to fire would originate from any location along the road network. This is because the road network passes through both major urban areas, as well as the rural communities, and therefore reflects the local population's ability to respond to fire in their area. The results from the cost-distance calculations were summed together, to create an overall friction surface. Finally, the friction surface was standardised by applying a simple linear membership function (Equation 21). The highest value in the friction surface was assigned a value of 1, linearly decreasing to 0, which was associated with the lowest friction values.

Table 4: Elevation friction values

Elevation (m)	Reclassified value
63 - 300	1
300 - 600	2
600 - 900	3
900 - 1200	4
1200 - 1500	5
1500 - 1800	6
1800 - 2113	7

Table 5: Land cover friction values

Land cover category	Reclassified value
Urban	1
Agriculture	3
Grassland	5
Low density forest	7
High density forest	10
River	15

Table 6: Slope friction values

Slope (°)	Reclassified value
0 - 5	1
5 - 10	2
10 - 15	3
15 - 20	4
20 - 25	5
25 - 30	6
30 - 35	7
35 - 40	8
40 - 45	9
45 - 73	15

$$\mu = \frac{\beta - x}{\beta - \alpha}$$

Equation 21

3.3.7. Formation of sub-models

The formation of each sub-model involves aggregating or combining the values in each raster layer to produce a single, final output. Operators such as fuzzy min and fuzzy max do not allow the analyst to account for the relative importance of different factors (section 1.3.3). For this reason, convex combination was used to assign weights to the factors of each sub-model (where applicable) to reflect their importance. However, a potentially subjective element of convex combination is that the assigned weights can be difficult to justify. To overcome this issue, a pairwise comparison was conducted, based on the analytical hierarchy process (AHP) of Saaty (1980). This method is advantageous because factors are both rated and compared against each other, before weights are derived. The rating system, which indicates how much more or less important a factor is with respect to another factor was based on findings from fire-related literature.

The pairwise comparison is performed in a matrix (Castellanos Abella and Westen 2007, Table 7). Criteria are placed on the vertical (A_1 to A_n) and horizontal axes (C_1 to C_n). Values that reflect the importance between factors are then assigned to each cell (e.g. cell a_{12} expresses the importance of factor A_1 against C_2). A value of 1/9 means that factor A1 is much less important than C2, while 9 is significantly more important (Saaty and Vargas 1991, Table 8).

The ratings in Table 7 are then normalised by dividing the value in a cell (e.g. a_{11}) by its column total (a_{11} by a_{m1}). This generates a new matrix in which each cell is assigned an Eigenvalue. The weights for each factor are derived by averaging the Eigenvalues in each row (a_{11} to a_{1n}). A consistency ratio (CR) is then calculated to

determine the success of the evaluation. The CR value should be less than 0.1 if consistency is good (Saaty 1980). If the CR is greater than 0.1 then the pairwise comparison should be re-evaluated. The equations used to calculate the CR can be found in Vadrevu *et al.* (2010).

Table 7: Matrix used in pairwise comparison

	C_1	C_2	...	C_n
A_1	a_{11}	a_{12}	...	a_{1n}
A_2	a_{21}	a_{22}	.	a_{2n}
.	.	.	.	.
A_m	a_{m1}	a_{m2}	...	a_{mn}

Table 8: Scale for pairwise comparison

Value	**Linguistic variable**
1	Equally important
3	Moderate prevalence
5	Strong prevalence
7	Very strong prevalence
9	Extremely high prevalence
2, 4, 6, 8	Intermediate values
Reciprocals	For inverse comparison

Formation of biophysical sub-model

The most important factor contributing to fire occurrence in a number of studies is land cover type. For example, Prasad *et al.* (2008) found that biomass density of land cover had the highest significance, among other factors, when a logistic regression was performed on a variety of factors (including elevation, aspect and slope). This is further supported by Lee *et al.* (2008, 197), where "fire severity was affected more by vegetation conditions rather than by topographic conditions". Land cover was also a "dominating influence on fire occurrence" in a study by Brosofske *et al.* (2007, 73). In Orozco *et al*. (2009), land cover was also given the greatest weight over elevation, slope and aspect.

Hammill and Bradstock (2006) found that aspect did not greatly influence fire behaviour, a result supported by Prasad *et al.* (2008) in their study of factors affecting fire occurrence. Elevation and slope are important in explaining fire occurrence, but it is not clear in the literature which has greater importance over the

other, although the two factors were found to be more significant than aspect (Rathaur 2006).

The above discussion of the relative importance of these factors was used to assign ratings to the different factors (Table 9). Weights were derived as shown in Table 9.

Table 9: Pairwise comparison for biophysical risk sub-model. CM: consistency measure; CI: consistency index; RI: random index; CR: consistency ratio

Rating	Land cover	Elevation	Slope	Aspect
Land cover	1.00	2.00	2.00	3.00
Elevation	0.50	1.00	1.00	2.00
Slope	0.50	1.00	1.00	2.00
Aspect	0.33	0.50	0.50	1.00
SUM	2.33	4.50	4.50	8.00

Weighting	Land cover	Elevation	Slope	Aspect	Average
Land cover	0.43	0.44	0.44	0.38	0.42
Elevation	0.21	0.22	0.22	0.25	0.23
Slope	0.21	0.22	0.22	0.25	0.23
Aspect	0.14	0.11	0.11	0.13	0.12

Factor	Weight	CM
Land cover	0.42	4.02
Elevation	0.23	4.01
Slope	0.23	4.01
Aspect	0.12	4.01

CI	0.003455
RI	0.9
CR	**0.003839**

Formation of ignition risk sub-model

Equal ratings were assigned to factors in the ignition risk sub-model. This is because articles studying the human factors affecting fire occurrence found distance from roads, and distance from land use types such as agriculture to be significant (Vasilakos *et al.* 2007; Vasconcelos *et al.* 2001). It is also important to note that prescribed fire is used both on agricultural land and grassland within this study area, meaning the likelihood of fire occurring in close proximity to these land cover types is greater. Equal ratings were used reflect the equal weight of each factor (Table 10).

Table 10: Pairwise comparison for ignition risk sub-model. CM: consistency measure; CI: consistency index; RI: random index; CR: consistency ratio

Rating	D. Agri	D. Grass	D. Roads		
D. Agri	1.00	1.00	1.00		
D. Grass	1.00	1.00	1.00		
D. Roads	1.00	1.00	1.00		
SUM	3.00	3.00	3.00		
Weighting	D. Agri	D. Grass	D. Roads	Average	CM
D. Agri	0.33	0.33	0.33	0.33	3.00
D. Grass	0.33	0.33	0.33	0.33	3.00
D. Roads	0.33	0.33	0.33	0.33	3.00
Factors	Weights				
D. Agri	0.33			CI	0.00
D. Grass	0.33			RI	0.58
D. Roads	0.33			**CR**	**0.00**

Formation of the weather sub-model

The CZI and temperature Z-scores must also be combined to produce 12 (monthly) outputs. The CZI was given greater rating because precipitation can have a more direct influence on fuel moisture content than temperature. When precipitation occurs, fuel is immediately dampened. Therefore months characterised by high precipitation (or high CZI value) are likely to have high fuel moisture, and a fire is unlikely to start even if the temperature is high. The rating and weighting of precipitation and temperature are shown in Table 11.

Table 11: Pairwise comparison for weather risk sub-model. CM: consistency measure; CI: consistency index; RI: random index; CR: consistency ratio

Rating	Precipitation	Temperature		
Precipitation	1	2		
Temperature	0.50	1		
SUM	1.50	3		
Weighting	Precipitation	Temperature	Average	CM
Precipitation	0.67	0.67	0.67	2.0
Temperature	0.33	0.33	0.33	2.0
Factor	Weight		CI	0.00
Precipitation	0.67		RI	0.00
Temperature	0.33		**CR**	**0**

Formation of the detection and response sub-models

The detection sub-model consisted of only one risk factor in the form of a viewshed analysis. Similarly, the response sub-model has one risk factor which was formed from the cost distance analysis. For both these sub-models it was therefore unnecessary to perform the pairwise comparison because there was nothing else in the sub-models to compare against.

3.3.8. Formation of final model outputs

The final outputs of the model were generated by performing a weighted combination of the sub-models. Twelve outputs were created, one for each month. The greatest rating was given to the weather sub-model, as weather exerts the most significant influence on fire occurrence. Hot and dry conditions between March and May gives rise to the area's fire season, while the monsoon between June and September reduces this occurrence. Prasad *et al.* (2008) also found that weather conditions, such as average temperature and precipitation, were significant in explaining fire occurrence. The biophysical sub-model was assigned the next highest rating, as land cover in particular affects where fire will burn. The ignition sub-model was assigned the third greatest weighting. Response and detection had the lowest ratings (Table 12).

Table 12: Pairwise comparison for combining risk sub-models. CM: consistency measure; CI: consistency index; RI: random index; CR: consistency ratio

Rating	Weather	Biophysical	Ignition	Response	Detection
Weather	1.00	2.00	3.00	4.00	5.00
Biophysical	0.50	1.00	1.00	2.00	3.00
Ignition	0.33	1.00	1.00	1.50	2.00
Response	0.25	0.50	0.67	1.00	2.00
Detection	0.20	0.33	0.50	0.50	1.00
SUM	2.28	4.83	6.17	9.00	13.00

Weighting	Weather	Biophysical	Ignition	Response	Detection	Average
Weather	0.44	0.41	0.49	0.44	0.38	0.43
Biophysical	0.22	0.21	0.16	0.22	0.23	0.21
Ignition	0.15	0.21	0.16	0.17	0.15	0.17
Response	0.11	0.10	0.11	0.11	0.15	0.12
Detection	0.09	0.07	0.08	0.06	0.08	0.07

Sub-model	Weight	CM
Weather	0.43	5.05
Biophysical	0.21	5.04
Ignition	0.17	5.05
Response	0.12	5.03
Detection	0.07	5.03

CI	0.00964
RI	1.12
CR	**0.0086**

3.3.9. Validation phase

Validation is an important process to undertake when any model is created. The model's results must be compared with the real world to determine the level of accuracy of its predictions (McKinion and Baker (1982) in Mayer and Butler (1993)). The validation burn scars were overlaid onto the final fire risk output and compared for April (highest risk month), September (lowest risk month), and February and November (approximately between the highest and lowest risk). The validation scars were also overlaid onto the static risk sub-models to assess performance.

The relative operating characteristic (ROC) was also used to provide an additional measure of model performance. Use of the ROC is advantageous when needing to express the quality of a model in terms other than percent. It assesses "the validity of a model that predicts the location of the occurrence of a class by comparing a suitability image depicting the likelihood of that class occurring [i.e. fire risk output] and a Boolean image showing where that class actually exists [i.e. validation burn scars]" (Eastman 2006).

3.3.10. Sensitivity analysis

The criteria weights used in the final weighted combination can still be a source of controversy or uncertainty. Sensitivity analysis (SA) "examines the extent of output variation of a model when input parameters are systematically varied" (Delgado and Sendra 2004, 1173). SA is therefore useful because it can be used to assess the robustness of results, and which parameters are most sensitive to change (Ravalico *et al.* 2010). In this study the SA method adopted by Chen *et al.* (2010) was used, whereby each sub-model's weight is varied one-at-a-time, whilst the other sub-model weights are held constant. The weight for each sub-model was adjusted in 2% increments between -20% and +20% (a total of 20 runs per sub-model). For each run, the total area occupied between risk categories (e.g. 0.5 - 0.6 etc.) was reported and presented in a graph.

4. RESULTS

The previous chapter described the methods used in this study. This chapter presents the results, and is structured in a way that relates these results to the order of the research objectives. The burn scar map is therefore presented first, followed by the results for each sub-model and their corresponding accuracies. The dynamic aspect of the model is then presented together with a measure of its performance. The results of the sensitivity analysis are last to be presented.

4.1. Burn scar map

790 burn scars were identified (Figure 24). Of these, a significant proportion was located in the national park area in the south and the central Terai plain. Fewer burn scars were located in to the north in the Churia Hills. Two different datasets were used to locate burn scars, namely an ASTER image, and a ALOS AVNIR-2 dataset. The overall classification accuracy of the ALOS AVNIR-2 dataset was 89% (Kappa = 0.7). It was not possible to obtain an accuracy assessment of the ASTER burn scars because they dated to 2008, and so would have been re-colonised by vegetation.

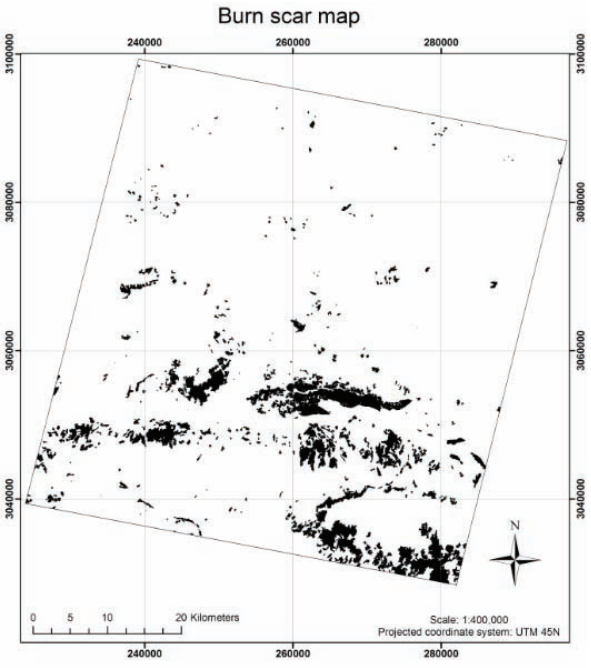

Figure 24: Burn scars located within the study area

4.2. Biophysical sub-model

In the case of the biophysical sub-model, the majority of the highest risk cells are located in parts of the study area covered by grassland (Figure 25), with the degree of risk approaching 1. Agricultural areas in the Terai plain are also at high risk, with values around 0.75. Lowest risk areas are found within the Churia Hills in the north of the study area, as well as in more inaccessible regions of Chitwan National Park. The effect of the fuzzy land cover boundaries is highly visible in regions of high risk, particularly land adjacent to agriculture and grassland (Figure 26). The effects of these fuzzy boundaries are less pronounced within the Churia Hills where the appearance of risk is more uniform. More than 70% of the burn scars are located in the 0.6 risk category and above, while few burn scars are located in risk areas of 0.4 or less (20%) (Table 13).

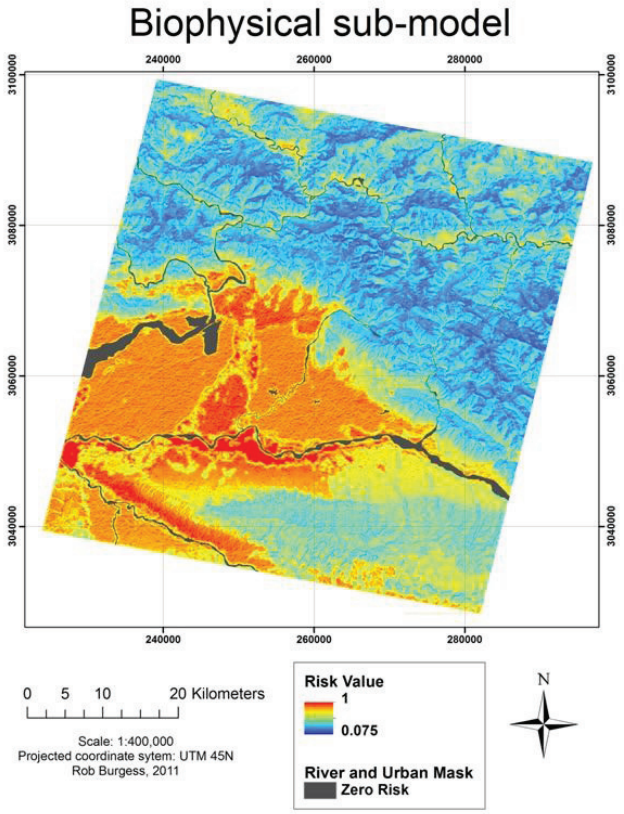

Figure 25: Biophysical sub-model fire risk map

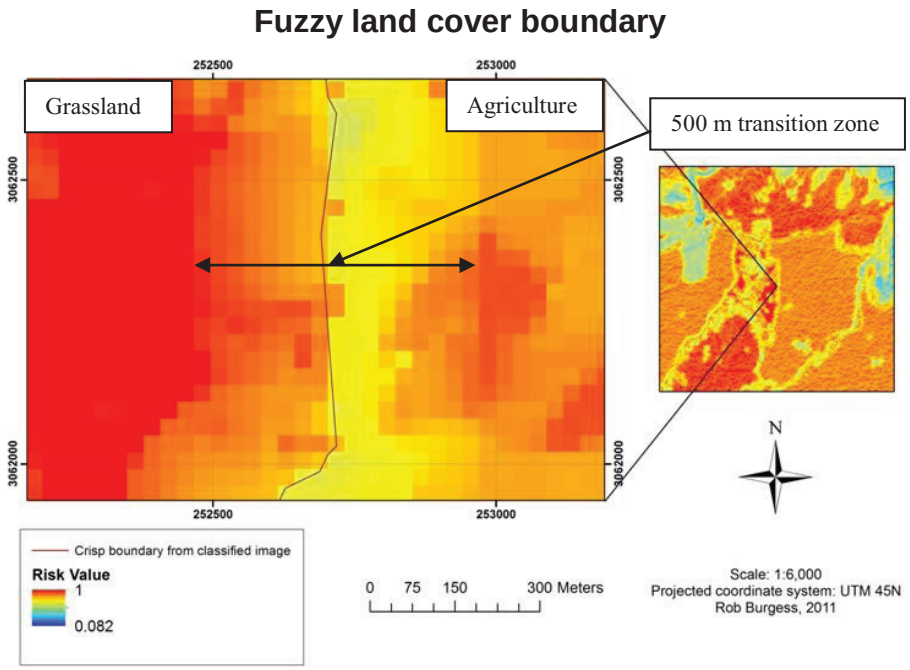

Figure 26: Effect of fuzzy land cover boundaries on risk of biophysical sub-model

Table 13: Performance of biophysical risk sub-model

Biophysical sub-model			
Risk	No. of scars	% of total scars	Cumulative %
1	7	1.78	1.78
0.9	26	6.60	8.38
0.8	137	34.77	43.15
0.7	73	18.53	61.68
0.6	46	11.68	73.35
0.5	39	9.90	83.25
0.4	41	10.41	93.65
0.3	25	6.35	100.00
0.2	0	0	100.00
0.1	0	0	100.00

Table 14: Performance of the ignition risk sub-model

Ignition sub-model			
Risk	No. of scars	% of total scars	Cumulative %
1	172	43.32	43.32
0.9	48	12.09	55.42
0.8	45	11.34	66.75
0.7	42	10.58	77.33
0.6	51	12.85	90.18
0.5	21	5.29	95.47
0.4	13	3.27	98.74
0.3	5	1.26	100.00
0.2	0	0.00	100.00
0.1	0	0.00	100.00

4.3. Ignition risk sub-model

In the case of the ignition risk sub-model, highest risk areas are situated within the Terai plain, with agricultural areas approaching the maximum level of risk (Figure 27). A corridor of high risk also exists in the northern part of the study area. Regions of the lowest risk occur in Chitwan National Park area in the south east, as well as parts of the Churia Hills. 43% of the burn scars are located within the highest risk category (Table 14), with more than 90% of the scars in the 0.6 category and above. Few scars are situated within the lower risk categories, with none occupying regions of 0.2 risk or less.

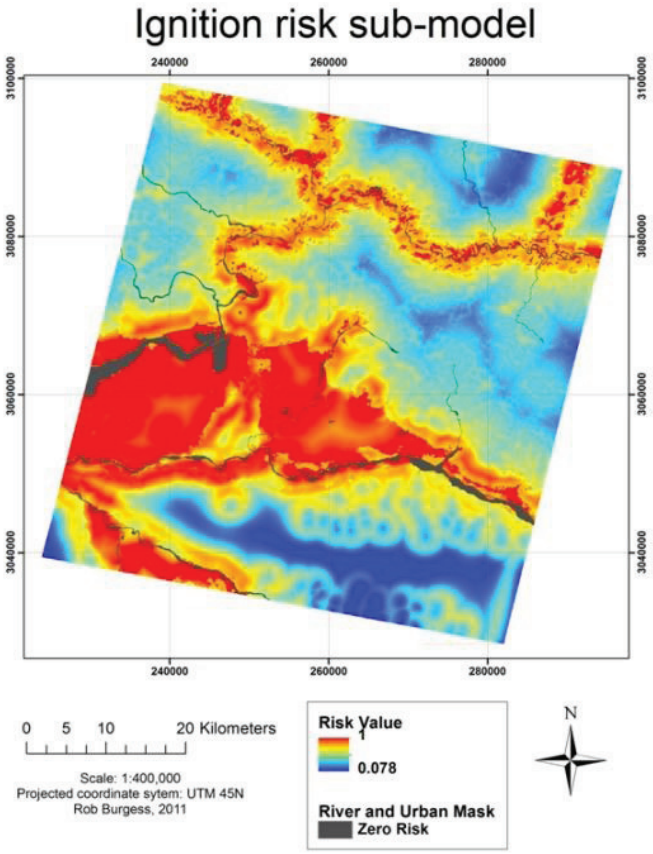

Figure 27: Ignition risk sub-model map

4.4. Weather risk sub-model

In the case of the dynamic weather risk sub-model, the highest and lowest risk months have been used to demonstrate the change in weather risk. In April, the risk values are highest, occupying a small range between 0.81 and 0.85, with the southern part of the study area occupied by these highest values (Figure 28). Conversely, September has the lowest risk values between 0.15 and 0.29 - a larger range compared to April.

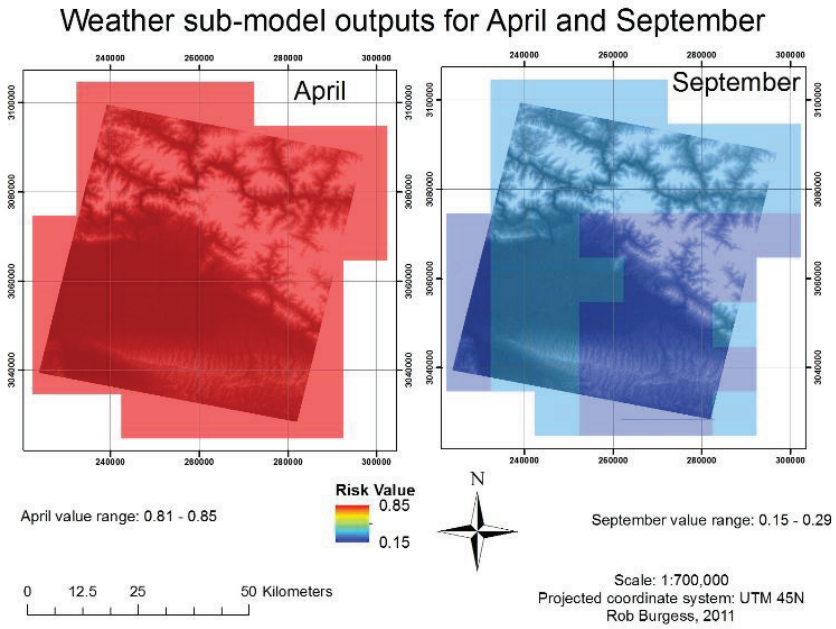

Figure 28: Two weather sub-model outputs depicting the risk in April and September, with DEM underneath.

4.5. Response sub-model

Areas at most risk to fire due to their inaccessibility include parts of Chitwan National Park, and eastern and western limits of the Churia Hills (Figure 29). Risk decreases as the proximity to roads increases, such that the imprint of the roads network is visible in the Terai plain, as well as a corridor running through the northern part of the study area. Interestingly, the majority of scars are located on regions of low risk. For example, nearly 60% of the burn scars are within the lowest risk category of 0 - 0.1, compared to approximately 2% of scars for the highest risk category (0.9 - 1.0) (Table15).

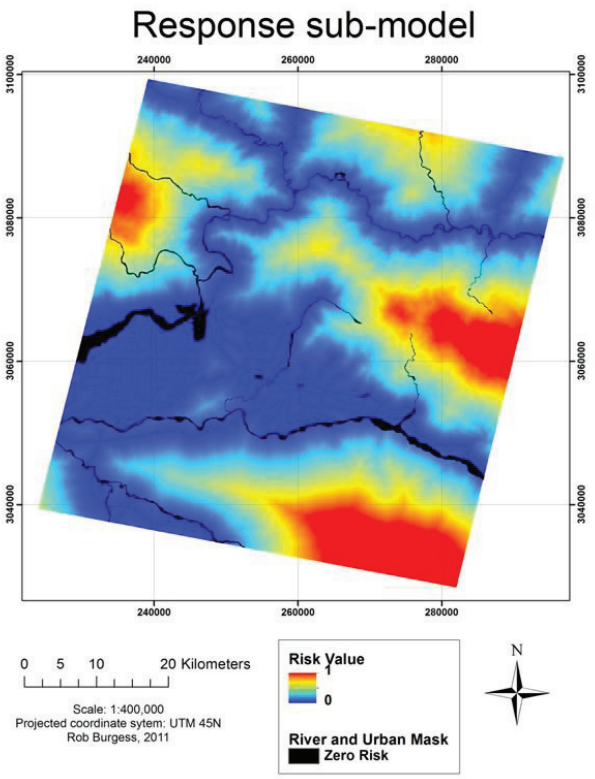

Figure 29: Response sub-model risk map

Table 15: Performance of the response sub-model

Response sub-model			
Risk	No. of scars	% of total scars	Cumulative %
1	9	2.31	2.31
0.9	11	2.82	5.13
0.8	8	2.05	7.18
0.7	12	3.08	10.26
0.6	8	2.05	12.31
0.5	21	5.38	17.69
0.4	19	4.87	22.56
0.3	27	6.92	29.49
0.2	46	11.79	41.28
0.1	229	58.72	100.00

Table 16: Performance of the detection sub-model

Detection sub-model			
Risk	No. of scars	% of total scars	Cumulative %
0.9	252	63.96	63.96
0.2	142	36.04	100.00

4.6. Detection sub-model

Visible areas are clustered around the existing road network (Figure 30). Large regions of the Terai plain are therefore at low risk (36% in total - Table 16). Beyond the 5 km visibility cut off land is invisible and hence high risk. 64% of the study area is categorised as high risk (Table 16).

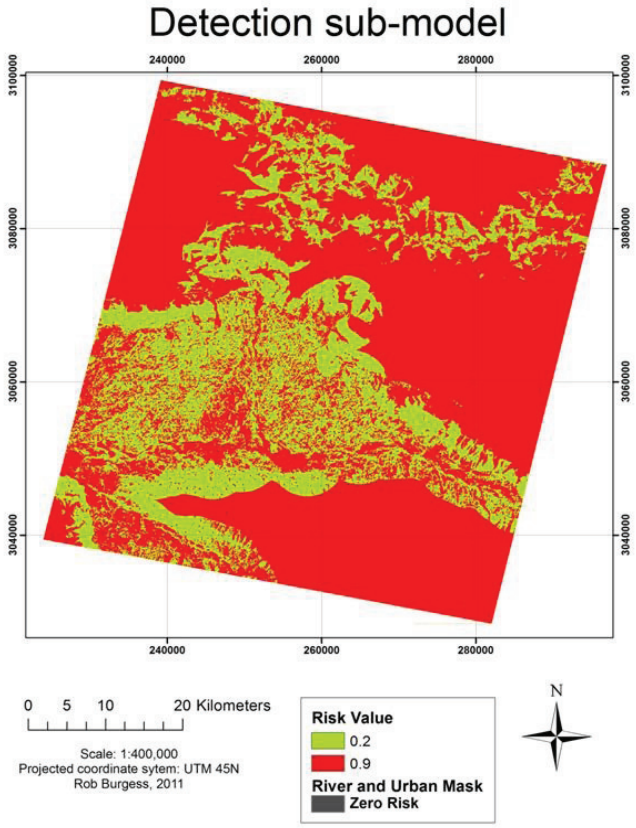

Figure 30: Detection sub-model risk map

Final monthly risk outputs

In the case of the final monthly risk outputs, 12 monthly scenarios were created using the outputs from the weather risk sub-model. Four of the outputs are presented in Figure 31 below. These correspond to the maximum risk for April, intermediate risk for February and November and minimum risk for September.

In each output, the degree of risk is always greatest in the Terai plain, approaching 0.83 in the month of April, and dropping to 0.57 in September. For February and November, risk is approximately midway between April and September at 0.75. Regions of lowest risk include parts of Chitwan National Park and a large proportion of the Churia Hills. See Appendix 7 to see risk outputs for each individual month. In the months characterised by low fire risk, sharp 'lines' can be seen in the images which appear to show abrupt changes in risk. This is caused by the coarse resolution of the climate data.

The change in risk from one month to the next can be seen in Table 17. In April, 97% of the burn scars are located in the 0.7 and 0.8 risk categories, indicating that this is the highest fire risk month. In February and November, the percentage of burn scars occupying the 0.8 risk category is less compared to that in April, shifting down to lower risk categories of 0.6 and 0.7. September is the lowest risk month with almost 90% of scars occupying the lower risk categories of 0.4 and 0.5. However, Table 17 also shows that within each month, the distribution of burn scars is narrow, occupying only 3 or 4 risk categories out of 10.

ROC curves in Figure 32 provide another measure of model performance, with each scenario being tested against a random model. Curves that are above the 'random model' line indicate a degree of success because the locations of the burn scars generally coincide with the areas of highest risk. Unsuccessful models would have a curve below the 'random model' line and an area under the curve (AUC) of <0.5 - in other words, the burn scars would be located in lower risk areas. Each month in Figure 31 is a reasonably good model, with April and February having the greatest AUC. September, the month at least risk to fire, had the lowest AUC of 0.7.

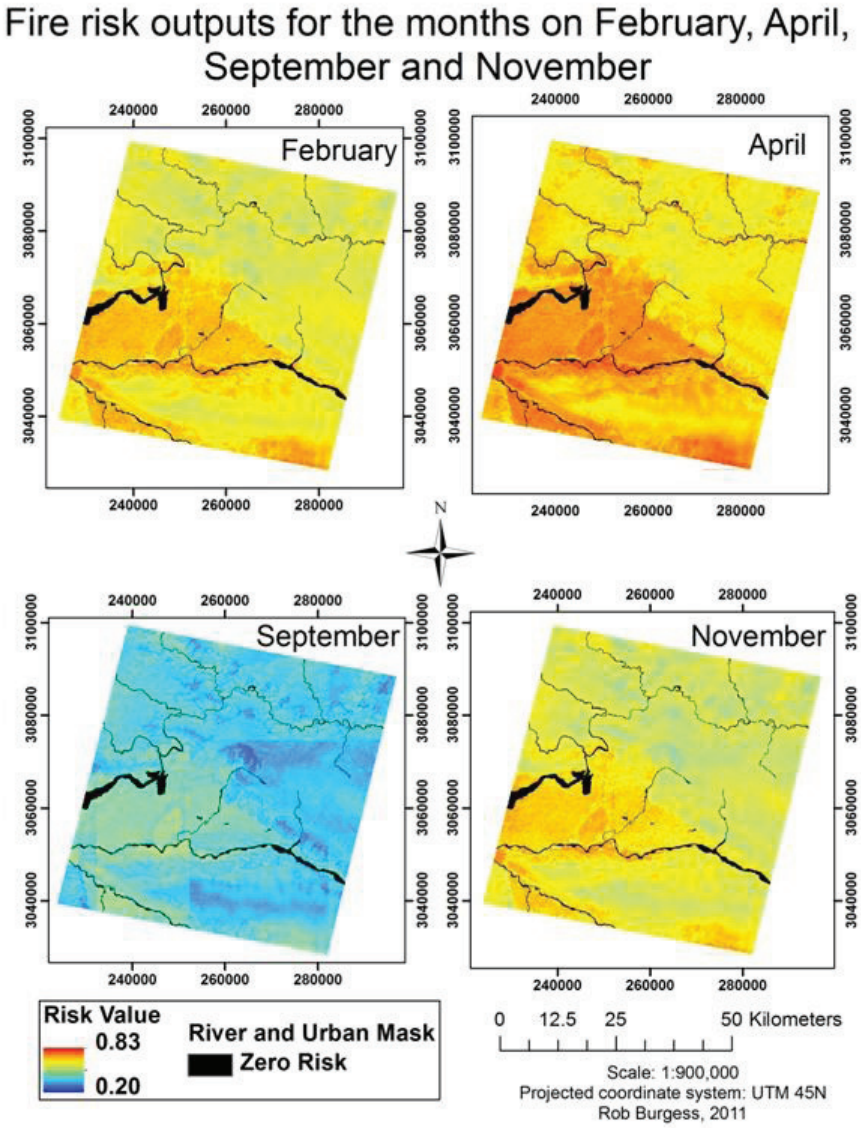

Figure 31: Risk maps for February, April, September and November

Table 17: Performance of four fire risk outputs

	Percentage of total no. of scars			
Risk	February	April	September	November
1.0	0.00	0.00	0.00	0.00
0.9	0.00	0.00	0.00	0.00
0.8	9.14	53.30	0.00	1.52
0.7	67.77	44.16	0.00	62.94
0.6	23.10	2.54	10.66	35.03
0.5	0.00	0.00	58.38	0.51
0.4	0.00	0.00	30.96	0.00
0.3	0.00	0.00	0.00	0.00
0.2	0.00	0.00	0.00	0.00
0.1	0.00	0.00	0.00	0.00

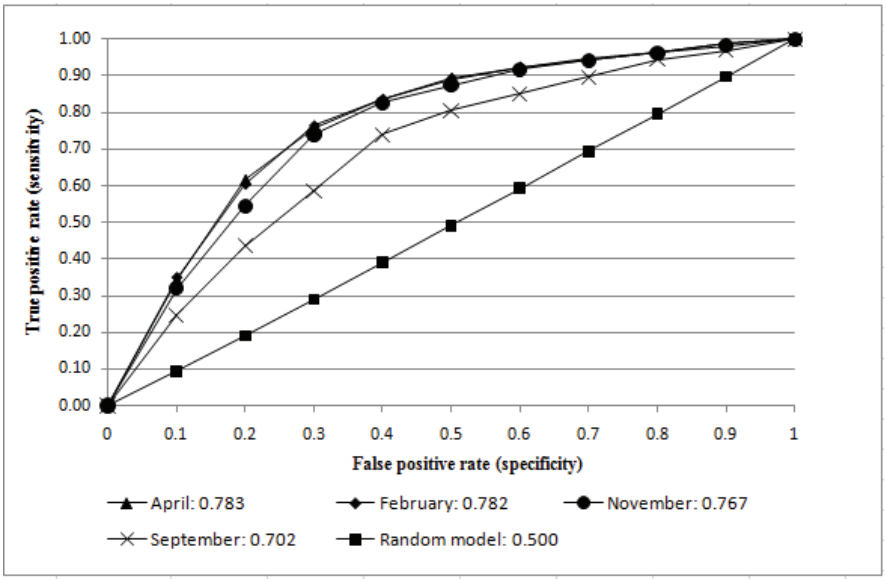

Figure 32: Relative operating characteristic (ROC) for four fire risk outputs

4.7. Sensitivity analysis

The results of the sensitivity analysis are summarised below. The graph for each sub-model is presented in Appendix 8. Each graph shows how the area contained within each risk category changes as the sub-model's weight is changed. The sensitivity analysis was performed on the month of April, chosen because this is the highest fire risk month.

- The **most sensitive** sub-model is the **weather sub-model**. As the weight is increased across the -20 to +20% range, the two categories that experience the most change are the 0.5 - 0.6 category, decreasing from 100,000 ha to near 0 ha, and the 0.7 - 0.8 category, increasing from 50,000 to 150,000 ha. The area within the 0.6 - 0.7 category appears to decrease both when the weight is increased and decreased.
- The **second most sensitive** sub-model is the **response sub-model**. The areas between the 0.5 - 0.6 and 0.7 - 0.8 categories converge as the weight is increased. As the weight is decreased from the original sub-model weight, the area contained within the 0.6 - 0.7 category decreases slightly, but is stable as the weight increases.
- For the **biophysical sub-model**, most change in area occurs between the 0.5 - 0.6 and 0.6 - 0.7 categories, which begin to converge as the weight increases.
- A slight increase in area from 75,000 to 100,000 ha is seen for the 0.7 - 0.8 category in the **ignition sub-model**. A gentle decrease occurs in the 0.6 - 0.7 category.
- The **least sensitive** sub-model is the **detection sub-model**, with minimal changes between the risk categories.

5. DISCUSSION

5.1. Burn scar map

Two major sources of data were used to locate burn scars within the study area, namely an ASTER image from which burn scars were *manually* digitised, and a burned area dataset from the ALOS AVNIR-2 sensor in which burned area had been detected *automatically*. Both methods have their advantages and disadvantages. Manual delineation of burn scars (a method used by Orozco *et al*. 2009 and Liew *et al.* 1998) is effective because the analyst is able to distinguish between burned area and land cover of a similar reflectance. However, in complex terrain such as the Churia hills located in the northern part of the study area, the presence of shadows can introduce a degree of uncertainty into burn scar identification.

The AVNIR-2 dataset is advantageous because the automatic detection of burned area can remove the subjective element associated with manual delineation, and data can be collected and used in near real-time (Roy *et al.* 2005). Burned area may also be identified in areas not visible to the human eye, but, again, it is important to note that land cover types of low/similar reflectance may still be classified as a burn scar (Sunuprapto 2000). The ground truth points collected in the field to assess the reliability of this dataset was, however, acceptably accurate, with 89% overall accuracy (Kappa = 0.7).

The use of these two data sources to provide a burn scar map does, however, introduce a degree of uncertainty into the calibration and validation phases. As mentioned in sections 3.1.2 and 4.1, no accuracy assessment for the ASTER image was available, whereas the AVNIR-2 dataset had an acceptable accuracy. This means that there is the potential for the calibration and validation of the fire risk model to be more or less accurate depending on whether the ASTER or AVNIR-2 data being used. This effect is therefore location specific because Chitwan National Park and the Terai plain are covered by the AVNIR-2 dataset, whereas a large proportion of the Churia hills are covered by the ASTER dataset. However, the magnitude of this effect was not possible to calculate because of the fact that the accuracy of the ASTER burn scars was not known.

A further issue arising from the use of these two datasets is that they were collected at two separate time periods (ASTER: March 2008, AVNIR-2: March 2010), and are therefore not subject to the same weather conditions. However, it was deemed important to use both these datasets because it made it possible to obtain burn scar

data that covered the whole study area, and these were also the most up to date datasets available.

5.2. Development of fire risk model

5.2.1. Biophysical sub-model

The majority of the highest risk cells are located in parts of the study area covered by grassland. This is an expected outcome due to the importance assigned to the land cover risk map (providing the fuel which fire burns), and because the greatest risk value (1.0) was originally assigned to grassland areas. In a similar risk study by Rathaur (2006) in northern India, the grassland cover type was also associated with the greatest fire risk, and may due to the similar climate and sub-tropical environment which these two study areas experience. However, the grassland is generally located in areas that are characterised by high risk in terms of slope (i.e. gentle slope) and elevation (i.e. low elevation). These results differ from the findings of Ercanoglu *et al.* (2006) because in this study, areas characterised by steep slopes were classified as higher risk. This is possibly due to the enhanced ability of fire to move upslope, as discussed in section 1.3.1. The result also differs from Hernandez-Leal *et al.* (2006) because in their study in Tenerife, regions of higher elevation were assigned greater risk values. This discrepancy could result from the different conditions that form wildfire regimes between study areas in very different locations.

The combination of slope and elevation is also important for explaining why agricultural land in the Terai Plain generally has high risk values, compensating for the 0.6 risk value originally assigned to the agricultural land cover category. The risk within agricultural areas is also affected by the aspect risk layer because the direction of the slope is continuously shifting across the Terai plain, which accounts for the 'speckled' appearance. The combination of low risk values for land cover, slope, elevation and in some cases aspect, accounts for the low risk areas of the Churia Hills region.

It is also important to discuss the impact of the fuzzy land cover boundaries on the biophysical sub-model, as their effect is highly apparent in regions characterised by high fire risk. Generally, the degree of risk in areas that fall within the fuzzy boundary zone is less than the risk value of pixels located outside these zones. Specifically, Figure 26 shows that the degree of risk gradually decreases as pixels

approach the crisp boundary as defined by the classified land cover map, accounting for the possibility that a pixel belongs to the adjacent land cover type. However, the fuzzy land cover boundary is limited because the risk suddenly decreases as the crisp boundary line is crossed from the grassland to agriculture side. Ideally, the risk values would continue to gradually decrease from the grassland to the agricultural land.

A further limitation of the method adapted from Lagacherie *et al*. (1996) to create fuzzy land cover boundaries also arises from when two or more land cover boundaries lie adjacent to each other. This is because the membership value of a pixel belonging to a land cover type decreases when there are possibilities that it belongs to other land cover types. If the membership value of the pixel to a land cover type is low, the resulting degree of risk also becomes lower when the two are multiplied. This has the effect of creating a much sharper decrease in risk values when comparing pixels within and outside the transition zone, giving it a less fuzzy appearance. Situations in which this occurs are generally located within the Churia Hills region, where the degree of risk is already low with respect to both slope and elevation.

The original positions of the crisp land cover boundaries, as well as the locations of some land cover polygons may also be affected by the supervised classification performed using the available GCPs. As mentioned in section 3.1.2., GCPs in the Churia Hills region were not collected randomly because of inaccessibility. The land cover map (and hence the boundary positions and location of the land cover polygons) would be different had it been possible to collect these GCPs randomly. Furthermore, the overall reliability of the land cover map, and accuracy of the fire risk model, would have improved had more GCPs per land cover type been collected. This is because the training stage of classification would have better represented the spectral signature associated with each land cover type, and the accuracy assessment would have been more thorough.

Sub-model performance was reasonable (Table 13), because 70% of the scars were located in the 0.6 risk category and above, while few were located in risk areas of 0.4 or less (20%). However, the biophysical sub-model developed by Orozco *et al*. (2009) appears to have performed better because the burn scars were not only located in areas that were classified as high risk, but were located in fewer risk categories. A reason for this may result from the differences in the Boolean and fuzzy approaches to standardisation and aggregation. In the Boolean approach adopted by Orozco *et al*. (2009) and Hernandez-Leal *et al.* (2006), risk values are

assigned to specific categories within a risk factor. For example, in Hernandez-Leal *et al.* (2006), a risk index value of 20 was assigned to all cells within 10 m of roads, 15 between 10 m and 50 m and so on. This creates distinct categories of risk similar to those discussed in section 1.4. If several risk factors are standardised in this way, it is likely that sharp boundaries between risk values will also be present in the final risk outputs. However, in the fuzzy approach, the gradual change from high to low risk limits these sharp changes in risk giving a much smoother appearance. When the two outputs are validated by seeing how the locations of the burn scars correspond to the risk maps, it is more likely that the scars will fit into a more compact number of categories when the Boolean approach is used. In the fuzzy approach, however, the location of the scar could be over a wider range of values.

A further possible reason why the biophysical sub-model did not perform as well as the biophysical sub-model in Orozco *et al*. (2009) could result from the application of the fuzzy membership functions in the standardisation process. Figure 9 in the methods chapter shows how a membership function was applied to the elevation histogram. The equation used is a single or 'global' function, designed to provide a best fit to the whole histogram. Although the use of one equation per risk factor is advantageous because it is simpler than breaking risk down into several smaller equations, the best fit aspect also means that there can be a degree of over- or underestimation of risk. Figure 9 shows a good example of overestimation of risk in the 1000 m bin category where there is a lower number of scars per ha relative to the 1200 m bin category, but has been assigned a greater degree of risk. The over- and underestimation is visible in the aspect histogram too (Figure 10), and also in some of the histograms in the ignition risk sub-model. This over- and underestimation of risk can propagate to the final sub-model output, adversely affecting its overall accuracy.

5.2.2. Ignition risk sub-model

The extensive road network located in the centre of the study area, and the area of grassland located on the northern border of Chitwan National Park explains the area of high risk in the Terai plain (Figure 27). The effect of the road is also visible in the northern part of the study area, creating the corridor of high risk. Regions of lowest risk are explained by significant distances from roads, grassland and agriculture.

The ignition sub-model performed better than the biophysical. 90% of the burn scars were located in the 0.6 category and above for the ignition sub-model (Table 14),

compared to 60% for the biophysical. This could indicate that the burn scars are in some way explained by human activities. Many fires ignite as a result of farmers deliberately setting fire to their fields in February and March to encourage growth of the next crop. In countries such as the US, Greece and Australia, arson can also be a significant issue. Although in Nepal there is no evidence to suggest arson is a problem, it remains possible that some fires may have started in this area because the road network provided easy access to particularly vulnerable areas. This is supported also by Romero-Calcerrada *et al.* (2008), who produced fire risk maps showing that, out of several human-caused wildfire ignition factors, the greatest danger was associated with proximity to roads. Finally, as mentioned in section 3.4.3, prescribed fire is sometimes used in grassland areas to support deer species which rely on young plants germinating from the burned area.

5.2.3. Response sub-model

When compared to the biophysical and ignition risk sub-models, the response sub-model produces near opposite results, with areas such as the Churia Hills and Chitwan National Park occupying regions of greatest risk. A high percentage of scars are located in low risk areas, meaning that authorities or communities concerned could respond relatively quickly to fire occurrence. The response risk map could also indicate the influence of the human population in igniting fires within close proximity to where they live.

5.2.4. Weather risk sub-model

The weather sub-model outputs produced for each month are successful because the values of risk vary throughout the year, reflecting the changing weather conditions. It produces results that would be expected: April is the highest risk month, which is traditionally in the middle of the fire season. August/September are the lowest risk months, which come towards the end of the monsoon season (Figure 28).

However, despite the weather risk sub-model producing reasonable results, it is still simplistic. Ideally, an index designed specifically to estimate the degree of fire risk would have been used rather than the use of a drought index which is based only on precipitation. One such index is the Keetch-Byram index for example, which is frequently used in parts of the US (Dolling *et al.* 2005). The degree of risk (between 0 and 800) is calculated using maximum temperature and precipitation totals. Unfortunately, this index could not be used in this study because daily weather data was not available, and there is also the issue of whether a fire index developed for

the US can applied to the Nepali context. The weather sub-model is also simplistic in the sense that only temperature and precipitation are relied on to estimate fire risk. In reality, wildfire occurrence is also affected by relative humidity, which controls fuel moisture content, and wind speed, which influences fire behaviour. If data to determine these variables were available in the study area, more complex, and realistic, fire risk indicators could be used. An example of such an index which uses all four of these weather components is the fire weather index (FWI) used by the Canadian Forest Service (Girardin and Wotton 2009).

5.2.5. Final monthly risk outputs

The final monthly risk outputs formed by the aggregation of the sub-models provides an insight into the spatial and temporal aspects of fire risk. The temporal change in risk is caused directly by the weather sub-model. However, the weather sub-model also has a degree of influence on the spatial distribution of risk, particularly in the lowest risk months. As can be seen in the September output of Figure 31, there are sharp changes in risk visible over the Churia Hills. This is caused by the spatial resolution of the weather data, which is coarse (10 km), meaning that any differences in risk between cells is easily visible. Furthermore, the differences in risk between cells in the monsoon season are much greater than the differences between cells in the fire season (e.g. Figure 28). This explains why such abrupt changes are only visible in the monsoon months.

Although the fire model is successful in showing the annual variation in risk (Table 17), the distribution or range of risk values between the extremes of April and September is not as great as expected. Ideally, lower risk values would have resulted for months such as August and September when the risk of fire probably approaches zero, rather than the 0.4 category shown for September in Table 17. Lower values in September would also have resulted in greater annual variation to the extent that changes in risk between months would have been more pronounced. The low range in risk values may be caused by different aspects of the multi-criteria evaluation approach adopted in this study. For example, many different factors, or risk sub-models, are being combined to produce one final output. This process of combination results in trade-offs between the different factors, as high risk areas in one factor can be partially compensated for by low risk elements of another. To an extent, this compensation between the risk sub-models is also affected by the weighting system, whereby weights were assigned to *a)* each factor map in the formation of each sub-model, and *b)* as weights used to combine the sub-models into the final risk outputs (Tables 9 to 12). At both stages, the weights are used to control

the degree of trade-off between factor maps. Increasing the weight of the weather sub-model, for example, would likely increase the range of values, particularly for months such as September when the risk would decrease further.

Despite this low range in values between April and September, use of the ROC demonstrated that model outputs are successful with AUC values ranging between 0.7 and 0.78. This does not mean that wildfires are likely to occur in the lowest risk months such as September just because it has a reasonable AUC value, but it does mean that throughout the year, the model is capable of distinguishing between areas of low and high risk. It also means that the land on which these validation burn scars occur remains consistently at high risk throughout the year relative to surrounding cells. In the study by Orozco *et al*. (2009), the ROC was also used to validate the fire risk model, achieving an AUC of 0.8. Although this value was obtained by validating a different aspect of the model (the static element of the model without the influence of weather), it does at least show some similarities and a degree of success common to both these studies.

5.2.6. Sensitivity analysis

The weights issue discussed above was also examined in a sensitivity analysis using the risk map for April. This month was chosen because it was the highest risk month of this study, and is traditionally in the middle of the fire season.

As summarised in the results chapter, the weather sub-model is the most sensitive to weight change as it exhibited the greatest changes in the distribution of risk. This is partly because the weather sub-model has the greatest weight over other sub-models and therefore has the greatest influence on the final risk values. It is also because of the coarse resolution of the weather sub-model (10 km), meaning that any change in its weight will result in broad and sudden changes in the risk values. Despite having the second lowest weight value, the response sub-model is the second most sensitive. This is explained by the location of the highest risk cells, which are situated over parts of the Churia hills and Chitwan National Park. This is in direct contrast to the location of highest risk cells in the biophysical, ignition risk and weather risk (April) sub-models. As the weight of the response sub-model is increased, it has a greater influence over these three sub-models, decreasing the values of the highest risk areas, and increasing the lowest. The detection sub-model was the least sensitive of the sub-models because it has the lowest weight.

The results of the sensitivity analysis indicate that, with the exception of the response sub-model, the sensitivity generally is greater with greater original weights. Chen *et al.* (2010) had broadly similar findings in an analysis of the weights used in an irrigated cropland suitability study. The sensitivity analysis also demonstrates the importance of the initial weights derived from the rating system in the pairwise comparison (section 3.4.3.), as the distribution and values of risk would differ if the rating values were changed. In the absence of expert opinion in deciding the initial weights, the sensitivity analysis is advantageous in that it can at least express how the result may have changed had the author chosen slightly different weights.

6. CONCLUSION AND RECOMMENDATIONS

6.1. Conclusion

A spatial and dynamic wildfire risk model based on fuzzy logic was developed for a region of southern Nepal. The general aim of the study was to identify regions most vulnerable to wildfire occurrence, and to ensure that the risk was realistic with respect to the temporal aspects of wildfire. Achieving this general aim was made possible by dividing it into four main objectives.

The initial objective, locating burn scars within the study area, was achieved by incorporating data from two different sources. The majority of this burn scar data was provided by an AVNIR-2 dataset from March 2010, while the remaining data was digitised using an ASTER image from March 2008. Although it is not ideal that these datasets were captured at different times using different approaches, it does provide data that covers the whole study area, as well as data on which to assess the spatial patterns of burn scars.

The histograms created by overlaying 50% of the burn scars with the factor maps enabled an assessment of their spatial patterns. This was an essential step in the achievement of the second objective, the development of the fire risk model itself. The histograms provided not only the values on which to base the fuzzy membership functions for risk, but the shape of the histograms provided guidance in the selection of a function's shape. Using these membership functions, the selected factors were successfully standardised to model the degree of risk.

Pairwise comparison was used in the formation of each sub-model that represented a particular theme of fire risk, and in the creation of the monthly fire risk outputs when the sub-models were combined. Ideally, expert opinion would have been used to decide the rating scores between the risk factors, but as this was not available, published literature was relied on. This introduces a degree of subjectivity with regard to the weights.

To address the third objective, the remaining 50% of the burn scars were used to assess the performance of each sub-model and each monthly risk output. The biophysical sub-model performance was reasonable in that 70% of the burn scars were located in the 0.6 risk category and above, but this is not as successful as a similar sub-model developed by Orozco *et al*. (2009). The ignition risk sub-model

was more successful in that 90% of scars were located in the 0.6 risk category and above.

The dynamic aspect of the model performed as expected. Fire risk was greatest for the month of April, which is also traditionally in the middle of the fire season, and was lowest in August and September, which experience high rainfall quantities as part of the monsoon season. However, the range of values between the maximum and minimum risk months are not as great as expected. Ideally, even lower values of risk values were expected for August and September. The reason risk is not lower is in part caused by the multi-criteria approach used in this study. Combining the sub-models can result in trade-offs, which acts to compensate against very high or very low risk values exhibited by a particular sub-model. The further method of validation using the ROC did, however, show that the final monthly outputs performed well, with an AUC above 0.7 to 0.78 for the months investigated.

A sensitivity analysis was performed by varying the weight of each sub-model in 2% increments between +20% and -20% of its original weight. Generally, greater original weights were associated with greater sensitivity - the weather sub-model was most sensitive, and the detection sub-model was the least. However, the response sub-model was also sensitive because the location of highest risk was in contrast to the other sub-models, demonstrating the importance of the trade-off influence between the sub-models. The sensitivity analysis also provided a degree of reliability against the subjective nature associated with the initial weights of each sub-model.

Finally, this study has shown the important contributions remote sensing and GIS can make to the spatial analysis and modelling of an environmental issue. In their absence, studies in regions of the world where little data is available would be a significant challenge, and the "white spot" remark which the IPCC made in relation to Nepal due to a lack of research done in this region, would persist (Khadka 2009). Instead, such techniques provide a powerful means of developing management strategies that can mitigate the negative impacts posed by such environmental issues.

6.2. Recommendations

Based on the results, discussion and conclusion in this study, the following recommendations are made.

- To improve the dynamic element of the fire risk model, select a study area in which several climate stations are located. This would provide not only ground measured data (i.e. not from a satellite estimate), but would also enable the possibility of incorporating the wind and relative humidity components into the model.

- In this study, monthly weather data between 2000 and 2010 were used, but only 2009 and 2010 was presented. It would therefore be possible to study the dynamic aspect of fire risk on a range of different time scales. For example, is there a particularly high risk period, and does this correspond to increased fire activity recorded in other datasets? Furthermore, the latest temperature and precipitation data could also be used to provide a recent assessment of risk.

- Increase the temporal resolution of the dynamic weather sub-model. Weekly and daily estimates may be more useful to fire managers/forestry officials, and would be relatively simple to achieve if climate stations were present in the area.

- The climate data could also be used to develop a fire index (e.g. similar to the Keetch-Byram index) rather than use of a drought index.

- More work needs to be done on the fuzzy land cover boundaries to make them more realistic. Alternatively, it might be interesting to incorporate a soft-classified image to provide a more fuzzy land cover layer, even if this does pose problems for accuracy assessment.

- Use of expert opinion would provide a robust and less subjective method for selection of fire risk factors and in deciding the weights used in combining these factors.

7. APPENDIX

Appendix 1: Materials description (Table 18)

Layer	Source	Description	Limitations	Justification of use
DEM	Land Processes Distributed Active Archive Center (LPDAAC) https://lpdaac.usgs.gov/lpdaac/get_data Accessed: 14/11/2010	**30 m ASTER** DEM.	Generated **without using GCPs**	Accuracy meets those specified in the Algorithm Theoretic Basis Document (ATBD) specified for absolute DEMs. More accurate than **25 m RMSExyz.**
ASTER image (land cover)	USGS Global Visualisation Viewer (GLOVIS). http://glovis.usgs.gov/. Accessed: 26/10/2010	Date of image: 21/02/2008. **15 m** resolution.	**3 bands used in classification**, which may be a limitation compared to sensors offering more bands.	Used because same sensor was also used to digitise burn scars.
Temperature	NASA Earth Observatories (NEO). http://neo.sci.gsfc.nasa.gov/Search.html. Accessed: 26/10/2010	**Land surface average daytime temperature** measured by MODIS instrument on the Terra satellite. 10 km spatial resolution. Monthly temporal resolution.	Limitations associated with the **radiative transfer methods and surface emissivity** used to estimate temperature. Resolution not ideal	**Too few climate stations within study area**, from which data was available only up to 2008. MODIS provides recent measurements (2010) that are accurate to within 1 K.
Precipitation	NASA Earth Observatories (NEO). http://neo.sci.gsfc.nasa.gov/Search.html. Accessed: 26/10/2010	Total monthly precipitation as detected by the Tropical Rainfall Monitoring Mission (TRMM) satellite. Spatial resolution of 0.25° (~**15 km**).	**Coarse resolution means that not many cells cover study area**. Also, TRMM sensors can fail to detect light rain or drizzle. Detecting rain over land surface more uncertain than over waterbodies.	**Too few climate stations within study area**, from which data was available only up to 2008.

Layer	Source	Description	Limitations	Justification of use
Roads layer	Data Repository of the Geographic Information Support Team. https://gist.itos.uga.edu/. Accessed: 26/10/2010. Road network also acquired using IPAQ and digitising from satellite image.	Both major and minor roads digitised within study area.	**Positional error** in IPAQ GPS may result in slight displacement of digitised road from actual road in some places, although in the majority of cases digitised and actual roads match.	Required for ignition risk, detection and response sub-models.
ALOS AVNIR-2	International Centre for Integrated Mountain Development (ICIMOD), Kathmandu, Nepal	Burned area as detected by **AVNIR-2** instrument on the ALOS satellite. **10 m** spatial resolution. Burned area is for **March 2010**	Approximately **40% of the study area is not covered** by the ALOS dataset, making it necessary to digitise burn scars present in this area.	ALOS dataset provides recent burn scar information. **Still covers a significant area of study area. Provides information that does not rely on human eye (digitising).**
MODIS detected ignition points	Fire Information For Resource Management System (FIRMS). http://maps.geog.umd.edu/firms/. Accessed: 26/10/2010	**Point shapefile** that indicates where thermal anomalies have been detected. These anomalies could potentially be fires, or sources of ignition.	In some cases, ignition points showed **no evidence of fire activity** when visited in the field.	Prior to receiving ALOS dataset, MODIS ignition points were **only source of possible fire activity.** Also provided extra source for burn scar map.

Appendix 2: Classified land cover map for study area

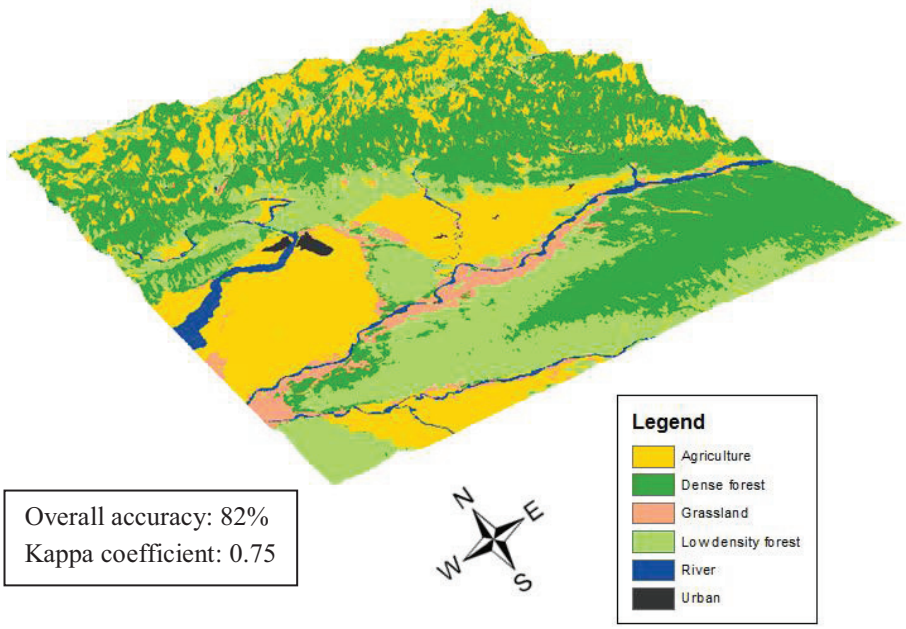

Appendix 3: Land cover accuracy assessment

	Ground truth (%)				
Class	D. forest	Grassland	L.D. forest	Agriculture	Total
D. forest	92.3	0.0	30.0	6.1	33.7
Grassland	0.0	75.0	5.0	3.0	14.7
L.D. forest	7.7	12.5	65.0	3.0	19.0
Agriculture	0.0	12.5	0.0	87.9	32.6
Total	100.0	100.0	100.0	100.0	100.0

Class	Comm. (%)	Omiss. (%)	Prod. Acc. (%)	User Acc. (%)
D. forest	25.0	7.7	92.3	75.0
Grassland	14.3	25.0	75.0	85.7
L.D. forest	27.8	35.0	65.0	72.2
Agriculture	6.5	12.1	87.9	93.6

Appendix 4: Examples of land cover types

Agriculture

Grassland

High density forest

Low density forest

Appendix 5: AVNIR-2 burned area dataset accuracy assessment

	Ground truth (%)		
Class	No burn scar	Burn scar	Total
No burn scar	100.0	33.3	78.3
Burn scar	0.0	66.7	21.7
Total	100.0	100.0	100.0

Class	Comm. (%)	Omiss. (%)	Prod. Acc. (%)	User Acc. (%)
No burn scar	13.9	0.0	100.0	86.1
Burn scar	0.0	33.3	66.7	100.0

Appendix 6: Histogram sensitivity analysis

Elevation (5, 10, 20 bins)

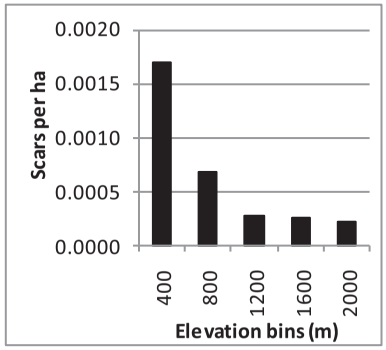

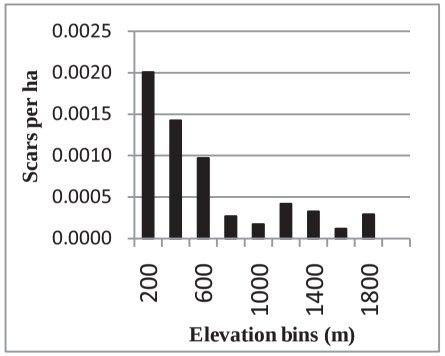

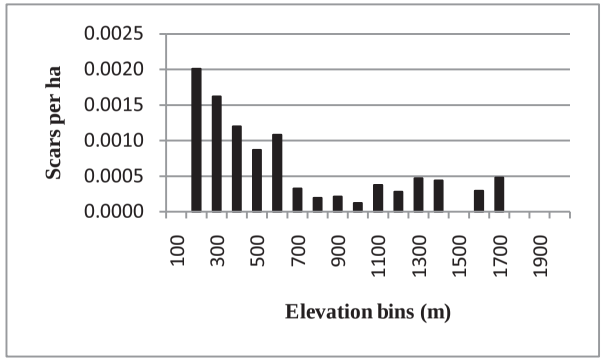

Aspect (9, 18, 36 bins)

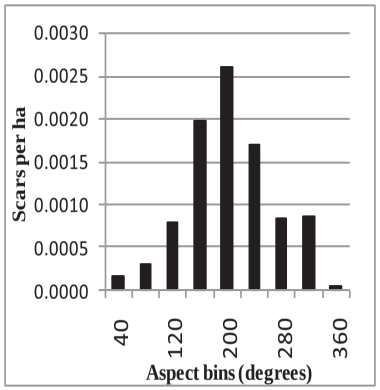

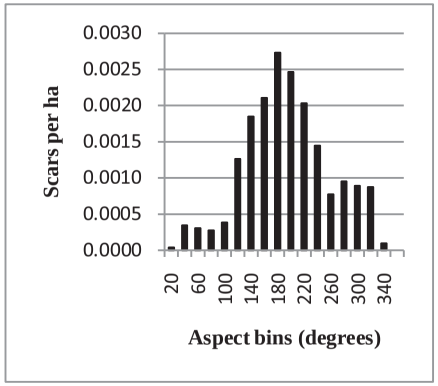

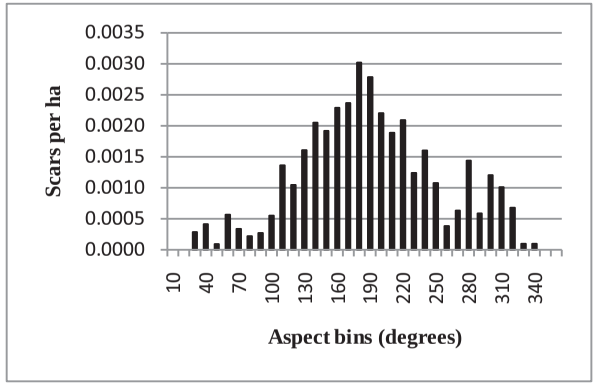

Slope (10, 20, 25 bins)

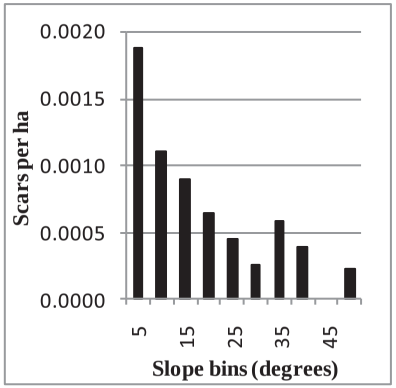

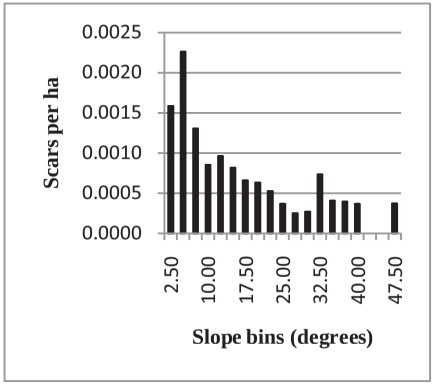

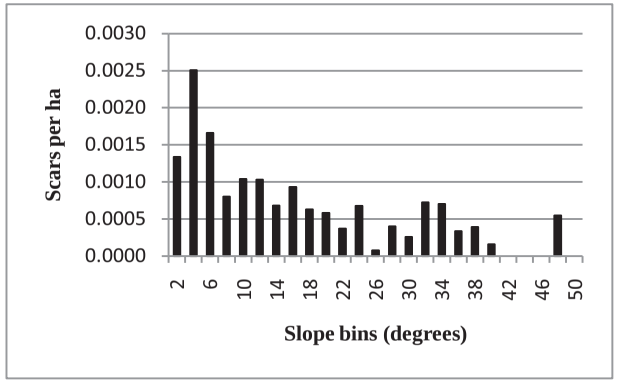

Distance from roads (10, 20, 40 bins)

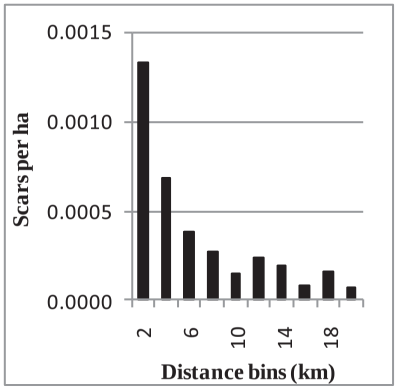

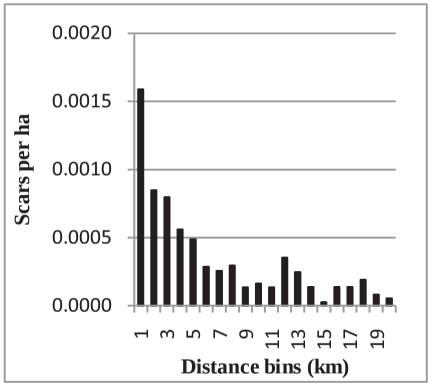

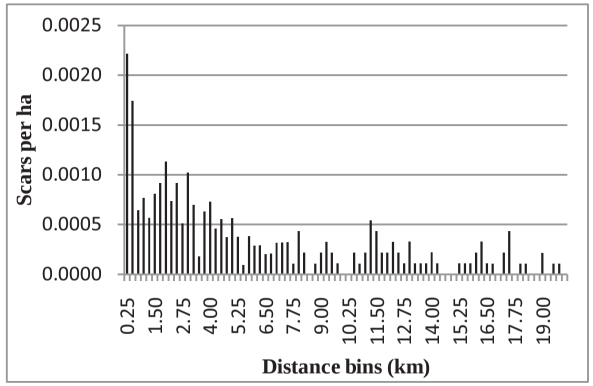

Distance from grassland (8, 12, 24 bins)

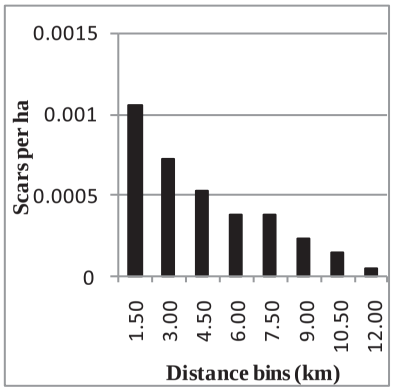

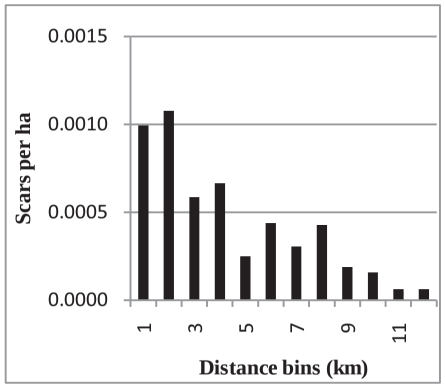

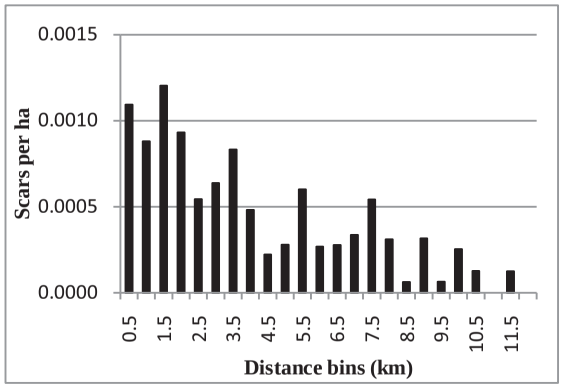

Distance to agriculture (7, 14, 28 bins)

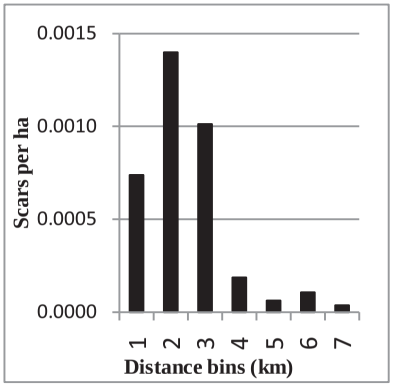

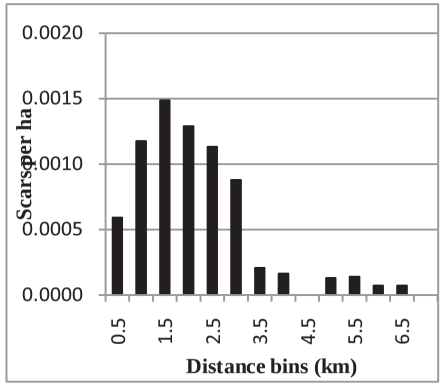

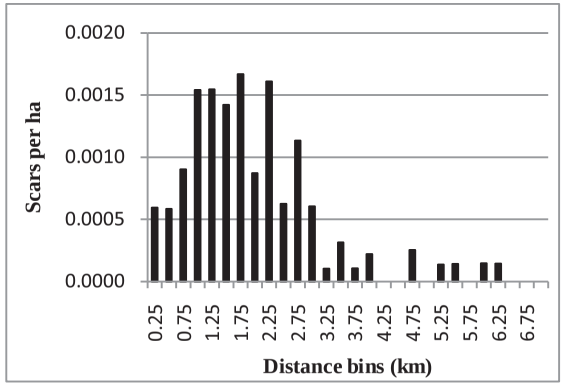

Appendix 7: Monthly risk outputs

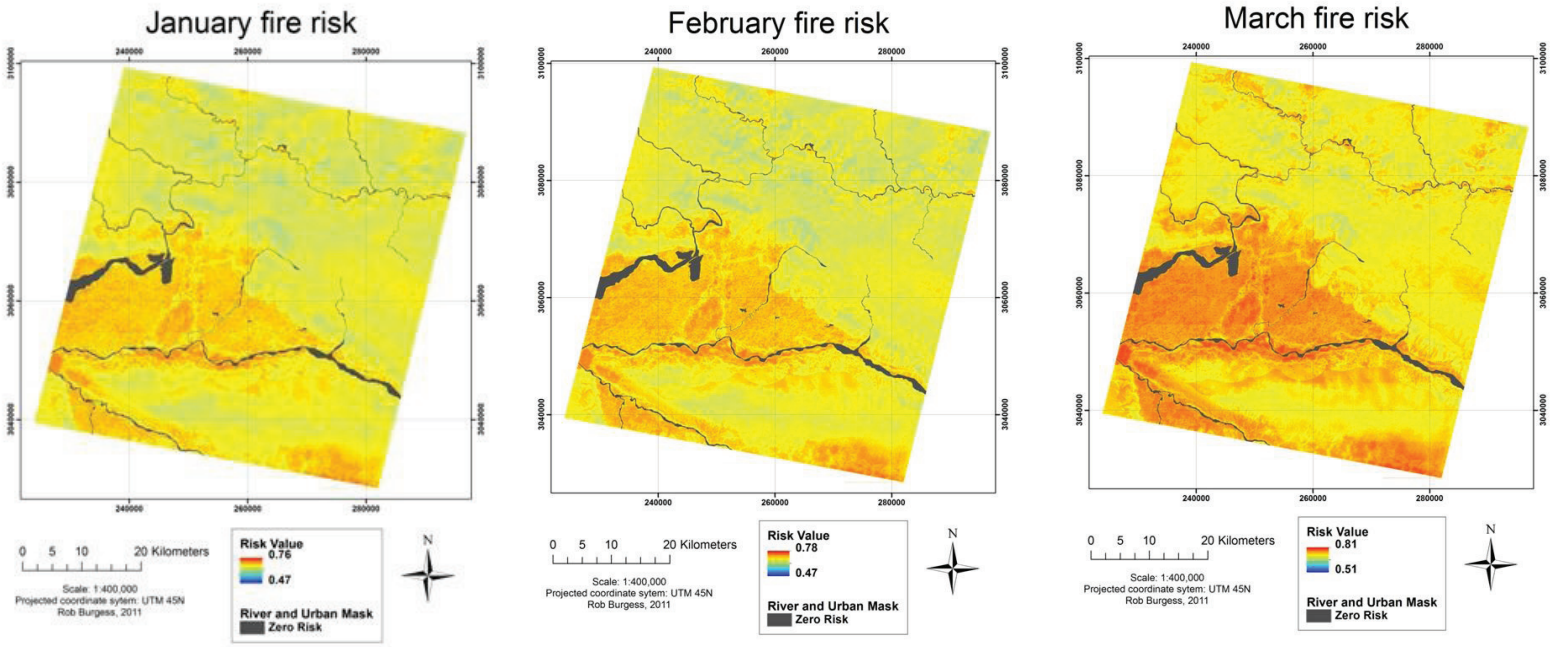

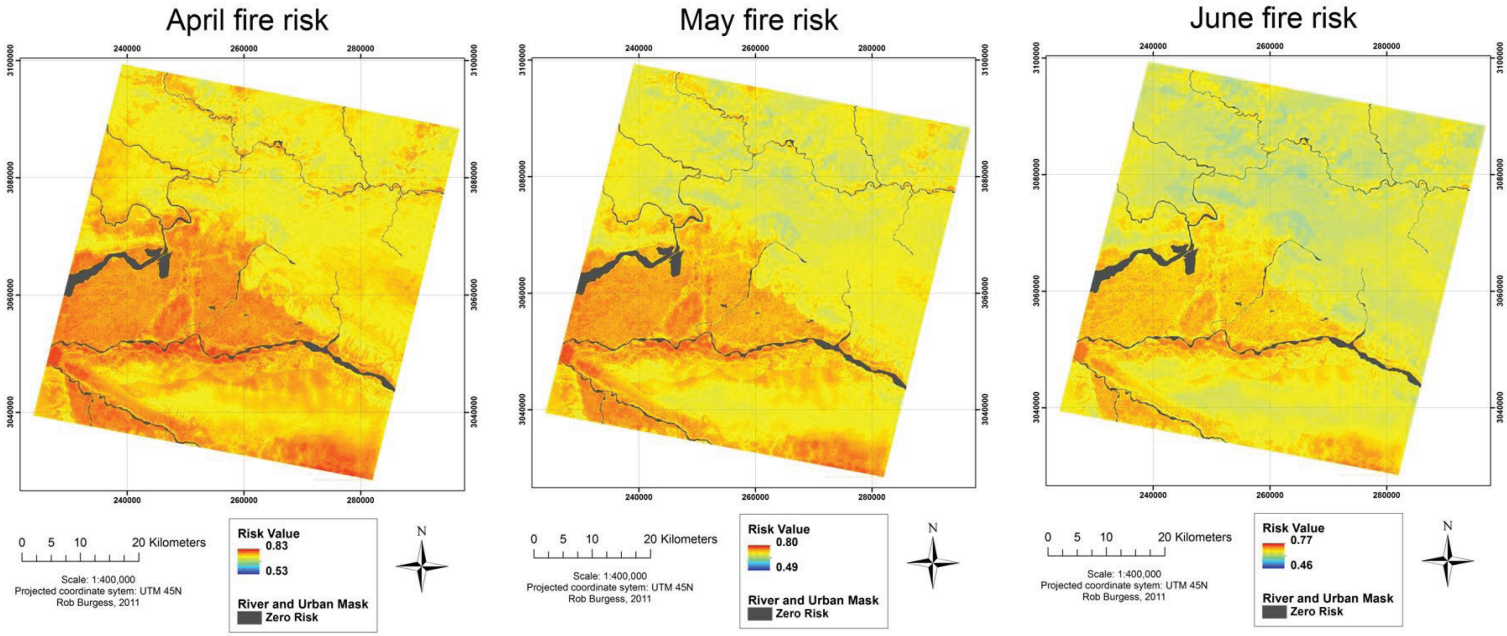
April fire risk
May fire risk
June fire risk
240000
260000
280000
3100000
3080000
3060000
3040000
0 5 10 20 Kilometers
Scale: 1:400,000
Projected coordinate sytem: UTM 45N
Rob Burgess, 2011
Risk Value
0.83
0.53
River and Urban Mask
Zero Risk
N
Risk Value
0.80
0.49
River and Urban Mask
Zero Risk
Risk Value
0.77
0.46
River and Urban Mask
Zero Risk

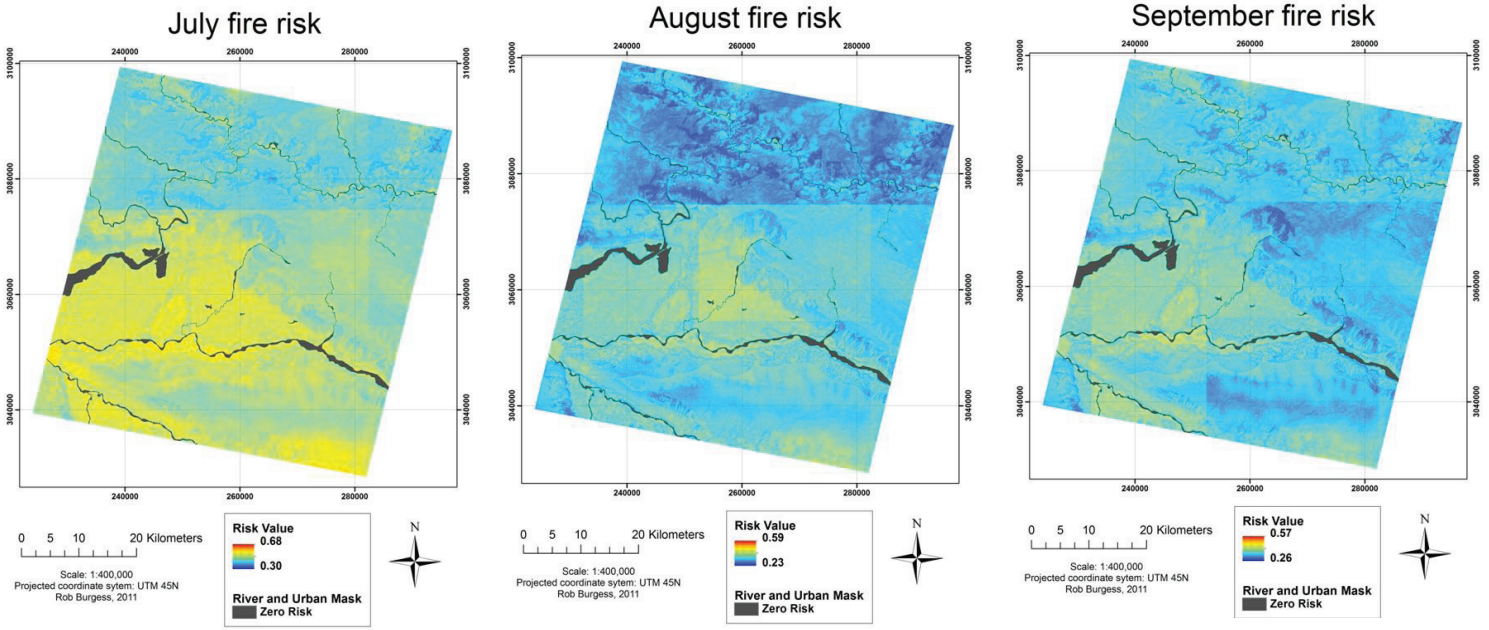
July fire risk
240000
260000
280000
3100000
3080000
3060000
3040000
0 5 10 20 Kilometers
Scale: 1:400,000
Projected coordinate sytem: UTM 45N
Rob Burgess, 2011
Risk Value
0.68
0.30
River and Urban Mask
Zero Risk
N
August fire risk
240000
260000
280000
3100000
3080000
3060000
3040000
0 5 10 20 Kilometers
Scale: 1:400,000
Projected coordinate sytem: UTM 45N
Rob Burgess, 2011
Risk Value
0.59
0.23
River and Urban Mask
Zero Risk
N
September fire risk
240000
260000
280000
3100000
3080000
3060000
3040000
0 5 10 20 Kilometers
Scale: 1:400,000
Projected coordinate sytem: UTM 45N
Rob Burgess, 2011
Risk Value
0.57
0.26
River and Urban Mask
Zero Risk
N

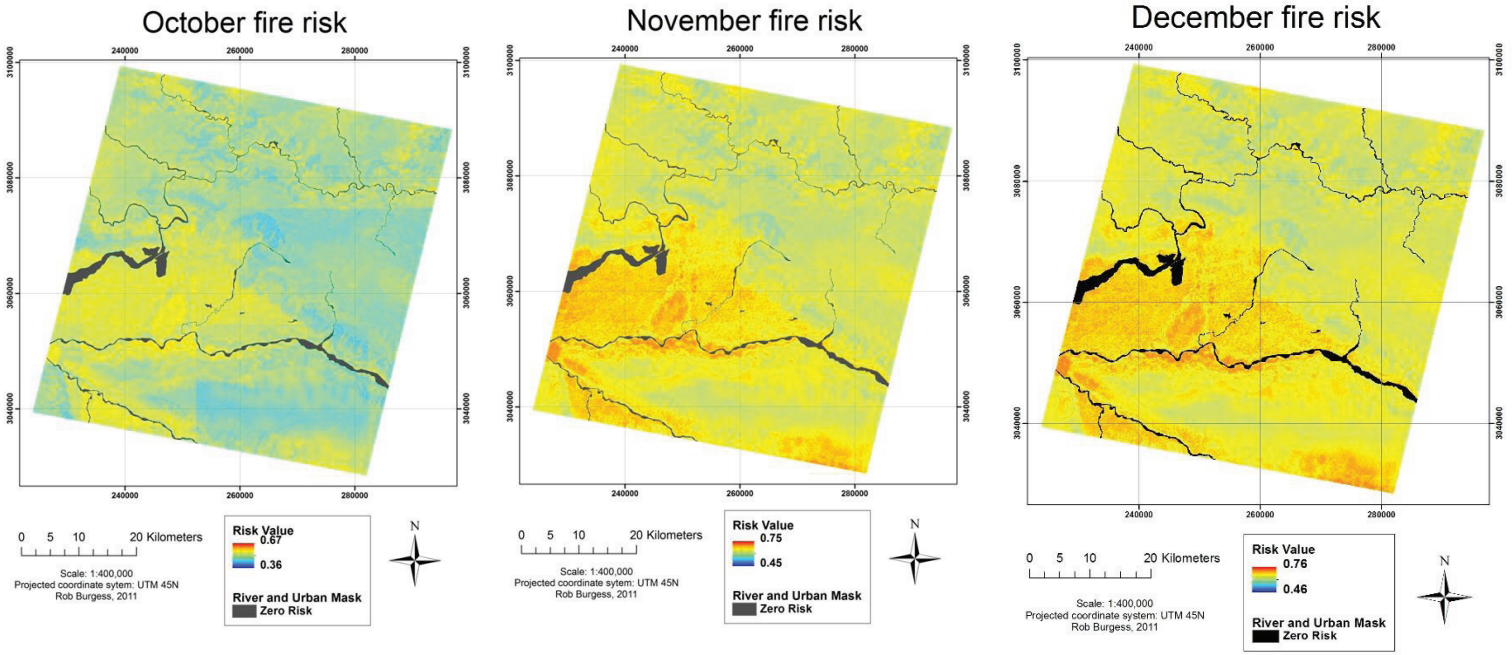
October fire risk
240000
260000
280000
3100000
3080000
3060000
3040000
0 5 10 20 Kilometers
Scale: 1:400,000
Projected coordinate sytem: UTM 45N
Rob Burgess, 2011
Risk Value
0.67
0.36
River and Urban Mask
Zero Risk
N
November fire risk
0.75
0.45
December fire risk
3080080
3060080
3040080
0.76
0.46

Appendix 8: Sub-model weight sensitivity analysis

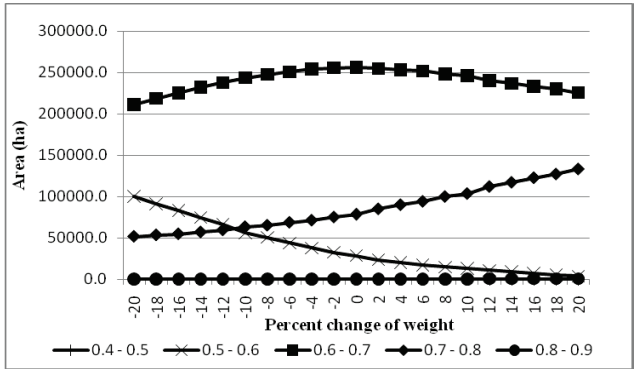

Sensitivity analysis of weather sub-model

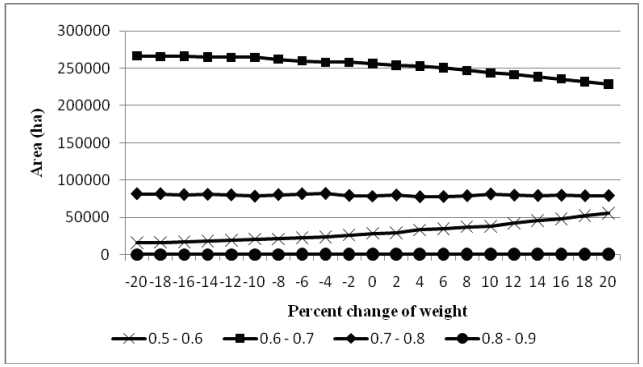

Sensitivity analysis of biophysical sub-model

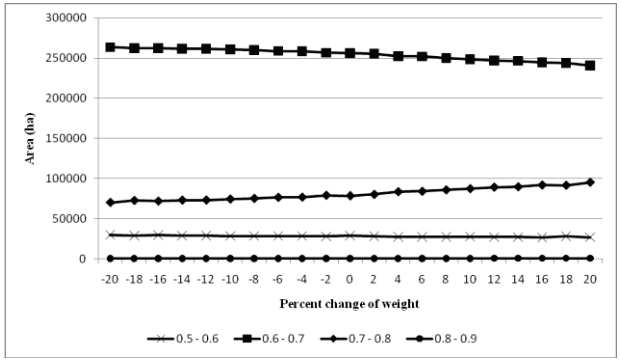

Sensitivity analysis of ignition risk sub-model

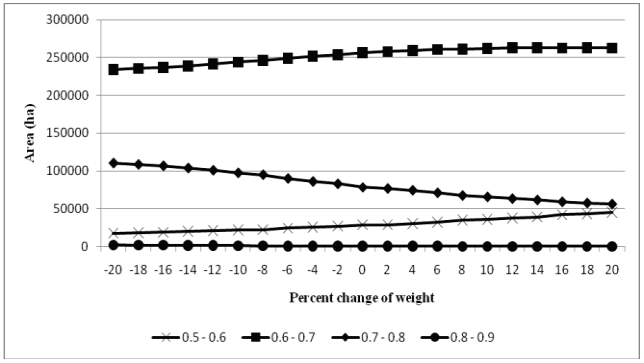

Sensitivity analysis of response sub-model

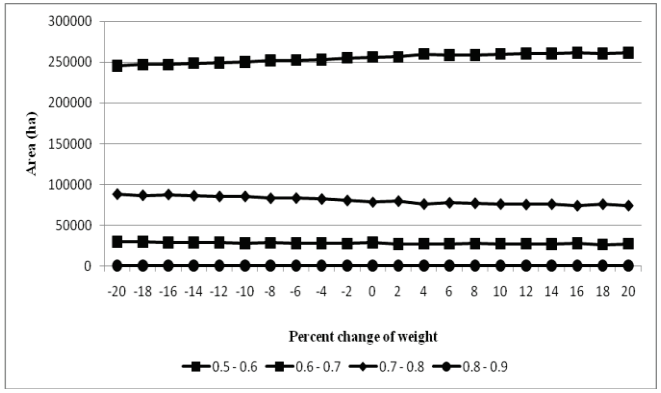

Sensitivity analysis of detection sub-model

8. REFERENCES

Acharya, K.B. and Dangi, R.B., 2009 [ONLINE]. *Case studies on measuring and assessing forest degradation. Forest degradation in Nepal: review of data and methods*, Rome. Available at: http://www.fao.org/docrep/012/k6869e/k6869e00.pdf. Accessed: 22/08/2010.

Albini, F.A., 1976. *Estimating wildfire behavior and effects*. General Technical Report INT-30. US Department of Agriculture, Forest Service, Intermountain Forest and Range Experiment Station, Ogden, UT, 1-100.

Amiro, B.D., MacPherson, J.I. and Desjardins, R.L., 1999. BOREAS flight measurements of forest-fire effects on carbon dioxide and energy fluxes. *Agricultural and Forest Meteorology*, **96**, 199-208.

ArcGIS 10 Help (2010). Using viewshed and observer points for visibility analysis. (Version 10): ESRI, Inc.

Bachmann, A. and Allgöwer, B., 2001. A consistent wildland fire risk terminology is needed! *Fire Management*, **61**(4), 28-33.

Bowman, M.J.S., Balch, J.K., Artaxo, P., Bond, W.J., Carlson, J.M., Cochrane, M.A., D'Antonio, C.M., DeFries, R.S., Doyle, J.C., Harrison, S. P., Johnston, F.H., Keeley, J. E., Krawchuk, M.A., Kull, C.A., Marston, J.B, Moritz, M.A., Prentice, I.C., Roos, C.I., Scott, A.C., Swetnam, T.W., van der Werf, G.R., and Pyne, S.J., 2009. Fire in the Earth System. *Science*, **324**, 481-484

Brosofske, K.D., Cleland, D.T., and Saunders, S.C. 2007. Factors influencing modern wildfire occurrence in the Mark Twain National Forest, Missouri. *Southern Journal of Applied Forestry*, **31**(2), 73-84.

Burrough, P.A., 1989. Fuzzy mathematical methods for soil survey and land evaluation. *European Journal of Soil Science*, **40**(3), 477-492.

Burton, I., and Kates, R. W., 1964. The perception of natural hazards in resource management. *Natural Resource Journal*, **3**, 412-441.

Butler, B., Forthofer, M., Finney, M., Bradshaw, L. and Stratton, R., 2006. *High resolution wind direction and speed information for support of fire operations.* Paper presented in the USDA Forest Service Proceedings RMRS-P-42CD, 595 - 602.

Castellanos Abella, E.A., and van Westen, C.J., 2007. Generation of a landslide risk index map for Cuba using spatial multi-criteria evaluation. *Landslides*, **4**, 311-325.

Cochrane, M. A., 2002 [ONLINE]. *Spreading like wildfire - Tropical forest fires in Latin America and the Caribbean: prevention, assessment and early warning*. Available at: http://desastres.usac.edu.gt/documentos/pdf/eng/doc16271/doc16271.htm Accessed: 19/01/2011.

Charnpratheep, K., Zhou, Q. and Garner, B., 1997. Preliminary landfill site screening using fuzzy geographical information systems. *Waste Management & Research*, **15**, 197-215.

Chen, K., Blong, R. and Jacobson, C., 2001. MCE-RISK: integrating multi-criteria evaluation and GIS for risk decision-making in natural hazards. *Environmental Modelling & Software*, **16**(4), 387-397.

Chen, Y., Yu, J. and Khan, S., 2010. Spatial sensitivity analysis of multi-criteria weights in GIS-based land suitability evaluation, *Environmental Modelling & Software*, **25**, 1582-1591.

Chuvieco, E. and Congalton, R., 1989. Application of remote sensing and geographic information systems to forest fire hazard. *Remote Sensing of Environment*, **29**(2), 147-159.

Chuvieco, E., 2000. Remote sensing of forest fires - current limitations and future prospects. In Observing land from space: science, customers and technology, Verstraere *et al.* (eds), Kluwer academic publishers, Netherlands, 47-51.

Chuvieco, E., Aguado, I. and Dimitrakopoulos, A.P., 2004. Conversion of fuel moisture content values to ignition potential for integrated fire danger assessment. *Canadian Journal of Forest Research*, **34**, 2284-2293.

Countryman, C.M., 1972. The fire environment concept. USDA, Forest Service. Pacific Southwest Forest and Range Experiment Station, Berkeley, California, pp12

Darwin, C., 1882 [ONLINE]. *The descent of man, and selection in relation to sex* - second edition. John Murray, London. Available at: http://darwin-online.org.uk/pdf/1882_Descent_F955.pdf. Accessed: 19/01/2011.

Delgado, M.G., and Sendra, J.B., 2004. Sensitivity analysis in multicriteria spatial decision-making: a review. *Human and Ecological Risk Assessment*, **10**, 1173-1187.

Dolling, K., Chu, P.S., and Fujioka, F., 2005. A climatological study of the Keetch/Byram drought index and fire activity in the Hawaiin Islands. *Agricultural and Forest Meteorology*, **133**, 17-27.

Dowmoh, F.K., Hussin, Y.A. and Oppong, K., 2009. *Spatial modelling of fire-induced carbon emission in tropical forests: A case study of Afram Head Waters Forest Reserve , Ghana*. Paper presented at the 2nd International Conference on Earth Observation for Global Changes - Chengdu, China. pp. 2159 - 2168.

Eastman, J.R., (2006). IDRISI Andes (Version 15). Worcester MA USA Clark Labs, Clark University

Ercanoglu, M., Weber, K.T., Langille, J., and Neves, R., 2006. Modelling wildland fire susceptibility using fuzzy systems. *GIScience & Remote Sensing*, **43**(3), 268-282.

Eva, H. and Lambin, E.F., 2000. Fires and land-cover change in the tropics: a remote sensing analysis at the landscape scale. *Journal of Biogeography*, **27**(3), 765-776.

FAO 1998 [ONLINE]. Country pasture / forage resource profiles. Available: http://www.fao.org/ag/AGP/AGPC/doc/Counprof/nepalhtm#3. , Accessed: 10/11/2010.

Fox, D.M., Maselli, F., and Carrega, P., 2008. Using SPOT images and field sampling to map burn severity and vegetation factors affecting post forest fire erosion risk. *Catena*, **75**, 326-335.

Finney, M.A., 1998. FARSITE: *Fire Area Simulator — model development and evaluation*. Research Paper RMRS-RP-4. US Department of Agriculture, Forest Service, Intermountain forest and Range Experiment Station, Ogden, UT.

Flannigan, M.D., Stocks, B.J., and Wotton, B.M., 2000. Climate change and forest fires. *The Science of the Total Environment*, **262**, 221-229

Girardin, M.P., and Wotton, B.M., 2009. Summer moisture and wildfire risks across Canada. *Journal of Applied Meteorology and Climatology*, **48**, 517-533.

Guttman, N.B, 1999. Accepting the Standardised Precipitation Index: a calculation algorithm. *Journal of American Water Resources Association*, **35**(2), 311-322.

Hardy, C.C., 2005. Wildland fire hazard and risk: problems, definitions, and context. *Fire Ecology and Management*, **211**, 73-82.

Heyerdahl, E.K., Brubaker, L.B. and Agee, J.K., 2001. Spatial controls of historical fire regimes: A multiscale example from the interior west, USA. *Ecology*, **82**(3), 660-678.

ICIMOD, 2010 [ONLINE]. Monitoring forest fires in Nepal ICIMOD. Available at: http://geoportalicimod.org/NAE/NewsDetail.aspx?mTab=homeandNLnk=newsandNewsID=225. Accessed: 08/09/2010.

Iliadis, L., 2005. A decision support system applying an integrated fuzzy model for long-term forest fire risk estimation. *Environmental Modelling & Software*, **20**(5), 613-621.

Jiang, H. and Eastman, J. R., 2000. Application of fuzzy measures in multi-criteria evaluation in GIS, *International Journal of Geographical Information Science*, **14**(2), 173-184.

Justice, C.O., Giglio, L., Korontzi, S., Owens, J., Morisette, J.T., Roy, D., Descloitres, J., Alleaume, S., Petitcolin, F., and Kaufman Y. 2002. The MODIS fire products. *Remote Sensing of Environment*, **83**, 244-262.

Kaufman, Y. J., Justice, C., Flynn, L., Kendall, J., Prins, E., Giglio, L., Ward, E.D, Menzel P. and Setzer, A., 1998. Potential global fire monitoring from EOS-MODIS, *Journal of Geophysical Research*. **103**(D24), 32215-32238.

Key, C.H., Benson, N.C., 2006. Landscape assessment: ground measure of severity, the composite burn index, and remote sensing of severity, the Normalised Burn Ratio. In: Lutes, D.C. *et al.* (Eds.), FIREMON. Fire effects monitoring and inventory system. USDA Forest Service Gen. Tech. Rep. RMRS-GTR-164-CD: LA1-51

Khadka, N. S., 2009 [ONLINE]. Climate change 'fans Nepal fires'. BBC. Available at: http://news.bbc.co.uk/2/hi/science/nature/7968745.stm. Accessed: 22/08/2010.

Lagacherie, P., Andrieux, P., and Bouzigues, R., 1996. Fuzziness and uncertainty of soil boundaries: from reality to coding in GIS. In Geographic Objects with Indeterminate Boundaries, Burrough, P.A., and Frank, A.U., (Eds.), Taylor and Francis, Great Britain, 275-286.

Lee, B., Kim, S.Y., Chung, J., and Park, P.S. 2008. Estimation of fire severity by use of Landsat TM images and its relevance to vegetation and topography in the 2000 Samcheok forest fire. *Journal of Forest Research*, **13**, 197-204.

Liew, S.C., Lim, O.K., Kwoh, L.K., and Lim, H., 1998. *A study of the 1997 forest fires in south east Asia using SPOT quicklook mosaics*. IGARSS '98 - 1998 IEEE International Geoscience and Remote Sensing Symposium, Seattle, WA; UNITED STATES, 879-881

Lu, D., Weng, Q., 2007. A survey of image classification methods and techniques for improving classification performance. *International Journal of Remote Sensing*, **28**(5), 823-870.

Martínez, J., Vega-Garcia, C. and Chuvieco, E., 2009. Human-caused wildfire risk rating for prevention planning in Spain. *Journal of environmental management*, **90**(2), 1241-52.

Matricardi, E. A. T., Skole, D. L., Pedlowski, M. A., Chomentowski, W. and Fernandes L. C., 2010. Assessment of tropical forest degradation by selective logging and fire using Landsat imagery. *Remote Sensing of Environment*, **114**(5), 1117-1129.

Mayer, D.G. and Butler, D.G., 1993. Statistical validation. *Ecological Modelling*, **68**, 21-32.

McBratney, A., B., and Odeh, I. O. A., 1997. Application of fuzzy sets in soil science: fuzzy logic, fuzzy measurements and fuzzy decisions. *Geoderma*, **77**, 85-113.

McKee, T.B., Doesken, N.J., Kleist, J., 1993. The relationship of drought frequency and duration to time scales. *Proceedings of the Eighth Conference on Applied Climatology*. American Meteorological Society, Boston, 197-184.

Mohammed, Y., Hussin, Y.A. and Sam, J.Q., 2009. *Modelling forest fire risk using remote sensing and GIS: A case study of transitional forest zone of Ghana*. Paper presented at the 2nd International Conference of Earth Observation for Global Changes - Chengdu, China.

Molders, N., and Kramm, G., 2007. Influence of wildfire induced land-cover changes on clouds and precipitation in Interior Alaska — A case study. *Atmospheric Research*, **84**(2), 142-168.

Morid, S., Smakhtin, V., and Moghaddasi, M., 2006. Comparison of seven meteorological indices for drought monitoring in Iran. *International Journal of Climatology*, **26**, 971-985.

National Wildfire Coordinating Group (NWCG), 2003 [ONLINE]. Glossary of wildland fire terminology. Available: http://www.nwcg.gov/pms/pubs/glossary/index.htm. Accessed: 21/12/2010

Ojha, H., Dahal, N., Baral, J., Subedi, R. and Branney P., 2008 [ONLINE]. Making REDD functional in Nepal: action points for capitalising opportunities and addressing challenges Discussion Paper (Draft). Available at: http://www.forestrynepalorg/images/publications/REDD%20discussion%20paper- Nepal-Dec%205-2.pdf. Accessed: 27/08/2010

Orozco, S.J., Hussin, Y.A., Weir, M., and Mas, J.F., 2009. *Modeling Fire Hazard and Control for Michoacán State, Mexico*. Paper presented at Proceedings of the 2nd International Conference on Earth Observation for Global Changes - Chengdu, China.

Palacios-Orueta, A., Chuvieco, E., Parra, A. and Carmona-Moreno, C., 2005. Biomass burning emissions: a review of models using remote-sensing data. *Environmental Monitoring and Assessment*, **104**(2), 189-209.

Pokharel, S., 2007. An econometric analysis of energy consumption in Nepal *Energy Policy*, **35**(1), 350-361.

Prasad, V.K., Badarinath, K.V. and Eaturu, A., 2008. Biophysical and anthropogenic controls of forest fires in the Deccan Plateau, India. *Journal of environmental management*, **86**(1), 1-13.

Prins, E.M. and Menzel, W.P., 1992. Geostationary satellite detection of biomass burning in South America. *International Journal of Remote Sensing*, **13**, 2783-2799.

Pyne, S. J., Andrews, P.L. and Laren, R.D., 1996. *Introduction to wildland fire* - second edition. John Wiley and Sons Inc, USA, pp 5-6

Rathaur, S., 2006. *Fire risk assessment for tiger prey-base in Chilla Range and vicinity, Rajaji National Park using remote sensing and GIS*, ITC MSc, Enschede.

Rautiainen, O. and Suoheimo, J., 1997. Natural regeneration potential and early development of Shorea robusta Gaertn.f. forest after regeneration felling in the Bhabar-Terai zone in Nepal. *Forest Ecology and Management*, **92**, 243-251.

Ravlico, J.K., Dandy, G.C., and Maier, H.R., (2010). Management Option Rank Equivalence (MORE) - A new method of sensitivity analysis for decision-making. *Environmental Modelling & Software*, **25**, 171-181.

Rein, G., Cleaver, N., Ashton, C., Pironi, P., Torero, J., 2008. The severity of smouldering peat fires and damage to the forest soil, *Catena*, **74**, 304-309.

Robinson, V.B., 2003. A perspective on the fundamentals of fuzzy sets and their use in geographic information systems. *Transactions in GIS*, **7**(1), 3-30.

Romero-Calcerrada, R., Novillo, C.J., Millington, J.D.A., and Gomez-Jimenez, I., 2008. GIS analysis of spatial patterns of human-caused wildfire ignition in the SW of Madrid (Central Spain). *Landscape Ecology*, **23**, 341-354.

Romme, W.H. and Knight, D.H., 1981. Fire frequency and subalpine forest succession along a topographic gradient in Wyoming. *Ecology*, **62**(2), 319-326.

Rothermel, R., 1972. *A mathematical model for predicting fire spread in wildland fuels*, Research Paper INT - 115. US Department of Agriculture, Forest Service, Intermountain forest and Range Experiment Station, Ogden, UT.

Roy, D.P., Jin, Y., Lewis, P.E., Justice, C.O., 2005. Prototyping a global algorithm for systematic fire-affected area mapping using MODIS time series data. *Remote Sensing of Environment*, **97**, 137-162.

Schroeder, M.J. and Buck, C.C., 1970. *Fire Weather and Fire Climate*, USDA Forest Service, Agricultural Handbook 360.

Schubert, P., 2004. *Cultivation potential in Hambantota District, Sri Lanka*. Lund University, Lund.

Scott, J.H. and Reinhardt, E.D., 2001. Assessing crown fire potential by linking models of surface and crown fire behavior. Research Paper RMRS-RP-29. US Department of Agriculture, Forest Service, Intermountain forest and Range Experiment Station, Ogden, UT.

Stickler, C.M., Nepstad, D.C., Coe, M.T., McGrath, D.G., Rodrigues, H.O., Walker, W.S., Soares-Filho, B.S. and Davidson, E.A., 2009. The potential ecological costs and cobenefits of REDD: a critical review and case study from the Amazon region. *Global Change Biology*, **15**(12), 2803-2824.

Sunuprapto, H. 2000. *Forest fire monitoring and damage assessment using remotely sensed data and geographical information systems (A case study in South Sumatra Indonesia)*. ITC MSc, Enschede.

Silván-Cárdenas, J.L. and Wang, L., 2008. Sub-pixel confusion-uncertainty matrix for assessing soft classifications. *Remote Sensing of Environment*, **112**, 1081-1095.

Timsina, N.P., 2003. Promoting social justice and conserving montane forest environments: a case study of Nepal's community forestry programme. *The Geographical Journal*, **169**(3), 236-242.

Thom, C.A., 2008. Community control of resources and the challenge of improving livelihoods: a critical examination of community forestry in Nepal *Geoforum*, **39**, 1452-1465.

Vadrevu, K.P., Eaturu, A. and Badarinath, K.V., 2010. Fire risk evaluation using multicriteria analysis - a case study. *Environmental monitoring and assessment*, **166**, 223-39.

Wrangham, R., and Carmody, R., 2010. Human adaptation to the control of fire. *Evolutionary Anthropology*, **19**, 187-199.

Wu, H., Hayes, M.J., Weiss, A., and Hu, Q., 2001. An evaluation of the standardised precipitation index, the China-Z index and the statistical Z-score. *International Journal of Climatology*, **21**, 745-758.

Yen, J., 1999. Fuzzy logic - a modern perspective. *IEEE Transactions on Knowledge and Data Engineers*; **11**(1), 153-165.

Zadeh, L.A., 1965. Fuzzy sets. *Information and Control*, **8**, 338-353.